Check for updates

ADVANCING EARTH AND SPACE SCIENCES

JGR Solid Earth

RESEARCH ARTICLE

10.1029/2025JB033218

Block Kinematics, Interseismic Coupling and Fault Slip Rates in the Aegean Region From GPS and Earthquake Slip Vector Data: 1. Upper Plate Structures

Konstantinos Chousianitis[1], Sotiris Sboras[1], Volkan Özbey[2], Robert McCaffrey[3], and Semih Ergintav[4]

[1]Institute of Geodynamics, National Observatory of Athens, Athens, Greece, [2]Department of Geomatics Engineering, Istanbul Technical University, Istanbul, Turkey, [3]Department of Geology, Portland State University, Portland, OR, USA, [4]Geodesy Department, Bogazici University, Kandilli Observatory and Earthquake Research Institute, Istanbul, Turkey

Key Points:

- We develop a block model to account for elastic strain accumulation along major upper plate faults and the subduction system
- We present estimates of slip rates, locking ratios, and slip rate deficits for the block-bounding upper plate faults
- The kinematic behavior of crustal blocks in the Aegean is governed by the complex interplay of large-scale plate tectonic interactions

Supporting Information:

Supporting Information may be found in the online version of this article.

Correspondence to:

K. Chousianitis,
chousianitis@noa.gr

Citation:

Chousianitis, K., Sboras, S., Özbey, V., McCaffrey, R., & Ergintav, S. (2026). Block kinematics, interseismic coupling and fault slip rates in the Aegean region from GPS and earthquake slip vector data: 1. Upper plate structures. *Journal of Geophysical Research: Solid Earth*, *131*, e2025JB033218. https://doi.org/10.1029/2025JB033218

Received 17 OCT 2025
Accepted 18 JUN 2026

Author Contributions:

Conceptualization: Konstantinos Chousianitis
Data curation: Konstantinos Chousianitis, Semih Ergintav
Investigation: Konstantinos Chousianitis, Sotiris Sboras
Methodology: Konstantinos Chousianitis, Volkan Özbey, Robert McCaffrey
Software: Konstantinos Chousianitis, Volkan Özbey, Robert McCaffrey
Supervision: Konstantinos Chousianitis
Visualization: Konstantinos Chousianitis
Writing – original draft: Konstantinos Chousianitis

© 2026. The Author(s).
This is an open access article under the terms of the Creative Commons Attribution License, which permits use, distribution and reproduction in any medium, provided the original work is properly cited.

Abstract We represent the active deformation of the Aegean region with an elastic-kinematic block model composed of a finite number of rotating crustal blocks whose boundaries coincide with major active structures. A total of 832 GPS velocities and 146 earthquake slip vectors were inverted to provide estimates of block rotations and interseismic locking on block-bounding faults so as to best reproduce the observed deformation field. Our regional model allowed us to derive a self-consistent set of geodetic slip rates for upper plate faults and the Hellenic subduction system, the results of which are presented in a companion paper, and to determine their corresponding slip rate deficits (geodetic moment accumulation rates). Most of the faults show either full or high levels of locking, with some exhibiting significant fault slip rate deficits, and only a few displaying very low or no coupling. Model results indicate that crustal blocks in the SE Aegean-SW Anatolia rotate counterclockwise, whereas those in central-NW Greece rotate clockwise. Between these domains, blocks move rapidly southwestward with trenchward-increasing velocities. The observed block motions in the Aegean reflect the combined influence of several large-scale tectonic processes that shape the present-day geodynamics, including the westward tectonic escape of Anatolia, rapid slab rollback and trench retreat along the Hellenic Arc, and along-strike variations in the Nubia-Eurasia plate boundary.

Plain Language Summary The Aegean region in the western Mediterranean is one of the most tectonically active areas in the world. To understand how the crust is deforming across the region, we divided the region into several crustal blocks separated by major faults. Using measurements from GPS stations and earthquake data, we estimated how these blocks move and how strongly the faults between them are locked or slipping. Our results show that many faults in the Aegean are mostly locked and accumulating strain in adjacent blocks, while a few are slipping more freely. We find that crustal blocks in southeastern Aegean and southwestern Turkey are rotating counterclockwise, while those in central and northwestern Greece rotate clockwise. Between these zones, crustal blocks move rapidly toward the southwest, with velocities increasing toward the Hellenic subduction zone. These deformation patterns reflect the combined effects of several large-scale processes; westward movement ("escape") of Anatolia, backward motion ("rollback") of the subducting slab beneath the Hellenic Arc, and variations along the boundary between the African (Nubian) and Eurasian plates. Together, these processes shape how the Aegean region moves and builds up the strain that drives its ongoing tectonic activity.

1. Introduction

The Aegean region of the eastern Mediterranean encompasses a complex and divergent tectonic environment which has been forged by the direct and indirect interaction between the Eurasian, Nubian, Arabian and Anatolian plates (Figure 1a). Throughout the paper we use the name "Aegean region" to refer to Greece and its adjacent regions to the east and north, namely the western coastline of Turkey and the southernmost part of the three Balkan countries that abut Greece. This region accommodates the ~NE-SW directed Nubian-Eurasian convergence and the westward lateral extrusion of the Anatolian plate relative to Eurasia along the North Anatolian Fault (NAF) which is induced by the northward movement of the Arabian plate (Jackson & McKenzie, 1984; Le Pichon & Angelier, 1979; Le Pichon & Gaulier, 1988; McClusky et al., 2000; McKenzie, 1972, 1978; Şengör, 1979). These first-order geodynamic mechanisms give rise to a number of second-order tectonic processes, such as the formation of active extensional grabens and the onset of strike-slip faulting (Armijo et al., 1999; Feng et al., 2010;

Writing – review & editing: Sotiris Sboras, Volkan Özbey, Robert McCaffrey, Semih Ergintav

Goldsworthy et al., 20002; Pérouse et al., 2017; Taylor et al., 2011; Taymaz et al., 1991; Vassilakis et al., 2011). As a result, the Aegean region is one of the most tectonically and seismically active areas globally. In this context, improved understanding of the deformation field and its mechanisms is crucial for gaining knowledge that will contribute to a more comprehensive evaluation of seismic hazard.

GPS-derived site velocities have been used in several previous geodetic studies in the Aegean region to quantify local and regional patterns and rates of tectonic deformation. Most of these studies used continuum models to describe the deformation field and interpreted the geodetic data by calculating and analyzing surface strain rates (Floyd et al., 2010; Hollenstein et al., 2008; Kahle et al., 2000; Kreemer et al., 2004; Pérouse et al., 2012). All of these studies have greatly increased our knowledge about the prevailing deformation processes, the accumulation of tectonic strain as well as its release rate through seismicity (Chousianitis et al., 2015, 2024; Jenny et al., 2004; Sparacino et al., 2022). However, there is still very limited, if any, available information on long-term fault slip rates and slip rate deficits for the several seismically hazardous active faults within the Aegean region. Estimation of these parameters, which provide the amount of the stored elastic strain energy along the faults, requires the utilization of methods that use a plate-like representation of the lithosphere. The observed deformation is represented as a combination of instantaneous block rotations and elastic strain rates due to interseismic locking along the block-bounding faults. Additionally, although the observed upper plate deformation in the Aegean region incorporates a component that is associated with subduction, very few studies took it into account (Barbot & Weiss, 2021; Vernant et al., 2014). In short, despite the fact that the Aegean region features many major active faults, our knowledge of their slip rates and their elastic strain accumulation is lacking.

Herein, we quantify the active deformation and develop a new kinematic framework for the present-day geodynamics of the Aegean region. Toward this end, we develop a block model and, using an up-to-date dense GPS velocity field and earthquake slip vectors, we estimate geodetic fault slip rates along the major seismogenic faults and assess their locking ratios. Additionally, we estimate the spatial variations of locking on the Hellenic subduction zone interface and on the Hellenic and Ptolemy trough splay faults that branch off the plate interface and accommodate some fraction of the Nubia/Eurasia convergence rate. In the present paper, we focus on the upper plate structures and, after analyzing the GPS velocity field and presenting the elastic block model, we estimate the kinematics of the tectonic blocks and derive a set of geodetic fault slip rates on the block-bounding faults. In the companion paper (Chousianitis et al., 2026), we present and analyze the results referring to the Hellenic subduction system (i.e., the plate interface and the Hellenic and Ptolemy trough faults). Both papers contribute to a better understanding of the crustal kinematics in the Aegean region and provide a refined quantification of the interseismic and long-term regional deformation.

2. Crustal Seismotectonics of the Aegean Region

The broader region of Greece displays a complex pattern of crustal deformation, which is driven by the convergence between the Eurasian and the Nubian plates and the propagation of the NAF across the Aegean Sea. Accordingly, the dominant lithospheric-scale tectonic structures of the Aegean region are the Hellenic subduction system and the NAF branches within the northern Aegean Sea. In the present paper we will not go into details on the Hellenic subduction system because it comprises the focus of the companion paper (Chousianitis et al., 2026), and we refer the interested reader there. As regards the dextral transcurrent NAF, it facilitates the westward escape of the Anatolian plate and contributes to the southwestward motion of the Aegean plate at ∼35 mm/yr, although this motion is also thought to be driven by additional processes such as slab rollback and gravitational potential energy contrasts (e.g., Allen, 1969; Hempton, 1982; Hatzfeld et al., 1997; McKenzie, 1972; Martinod et al., 2000; McClusky et al., 2000; Royden, 1993; Reilinger et al., 2006). The NAF's intrusion into the Aegean Sea probably took place ca. 5 Ma ago (e.g., Armijo et al., 1996, 1999; Barka, 1992; Şengör & Canitez, 1982) and today the two major tectono-morphological features which are associated with the westward continuation of the NAF, are the North Aegean Trough (NAT) and the North Aegean Basin (NAB) (Figure 1b). The NAT is a distinctive ENE-WSW trending scar on the seafloor of northern Aegean. As almost a pure shear structure, the uppermost part of the NAT is represented by a typical negative flower structure (McNeill et al., 2004; Roussos & Lyssimachou, 1991; Rodriguez et al., 2023; Yaltırak & Alpar, 2002) which has depressed the sea-bottom in its central part for almost 1,000 m. Pure shear turns gradually into transtension westwards, along the adjacent NAB, before it finally changes into approximately N-S oriented extension continuing to the western margin of the basin (Sboras et al., 2017 and references therein; Chousianitis et al., 2024). A smaller quasi-parallel and less prominent basin is located south of the NAT and the NAB; the Skyros Basin (SB in Figure 1b). The SB is a similar, less distinctive

21699356, 2026, 7, Downloaded from https://agupubs.onlinelibrary.wiley.com/doi/10.1029/2025JB033218, Wiley Online Library on [04/07/2026]. See the Terms and Conditions (https://onlinelibrary.wiley.com/terms-and-conditions) on Wiley Online Library for rules of use; OA articles are governed by the applicable Creative Commons License

21699356, 2026, 7, Downloaded from https://agupubs.onlinelibrary.wiley.com/doi/10.1029/2025JB033218, Wiley Online Library on [04/07/2026]. See the Terms and Conditions (https://onlinelibrary.wiley.com/terms-and-conditions) on Wiley Online Library for rules of use; OA articles are governed by the applicable Creative Commons License

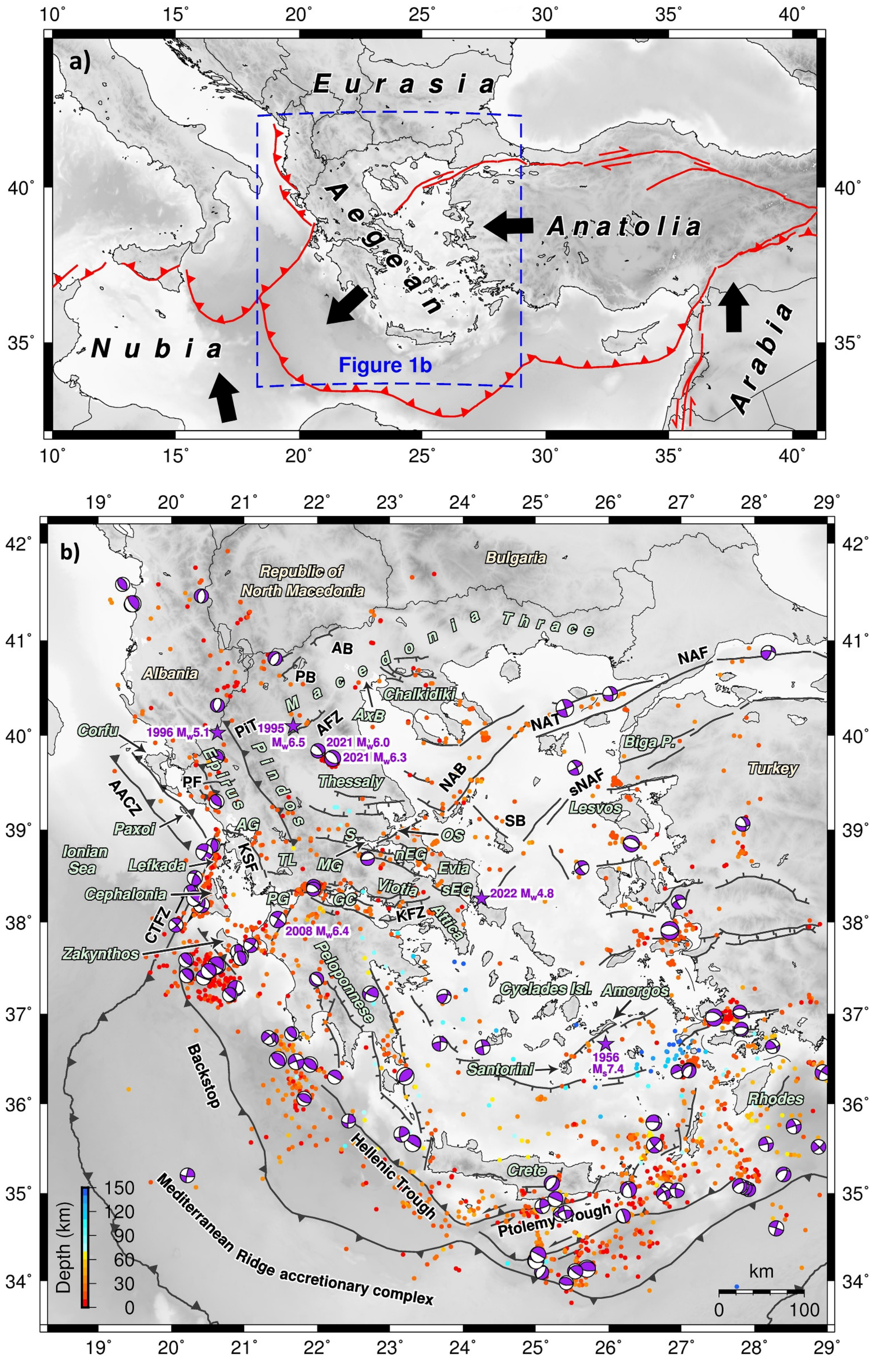

Figure 1.

tectonic system which is formed by the southern branch of the NAF (sNAF in Figure 1b) that crosses the Biga peninsula in Turkey and enters the Aegean NW of Lesvos island. The seafloor morphology is less developed with shallower depths than its similar trench and basin system to the north, implying diminished activity.

Another prominent structure that is associated with intense and frequent seismic activity is the dextral strike-slip Cephalonia Transform Fault Zone (CTFZ). It is located at the western end of the Hellenic subduction system and separates the Nubian/Aegean convergence zone to the south from the continental subduction and collision of the Aegean and Apulian plates to the north (Pearce et al., 2012). The CTFZ runs offshore, parallel to the western coasts of Cephalonia and Lefkada islands, forming a prominent underwater scarp which reaches a depth of approximately 3,000 m. The formation of this transform fault zone is due to differences in convergence (~35 mm/yr) and collision rates (5–10 mm/yr) south and north of the CTFZ respectively, as well as to different slab composition. It is interpreted as lateral ramp (Shaw & Jackson, 2010) or as a Subduction-Transform Edge Propagator (STEP) fault (Özbakır et al., 2020). The Aegean-Apulian Collision Zone (AACZ) is directly north of the northeastern end of the CTFZ with the Aegean plate overriding the Apulian plate. It forms a distinctive scarp on the seabed west of the Paxoi and Corfu islands, in the northern Ionian Sea. The thrust beneath the seabed sediments has been detected in seismic tomography studies (Halpaap et al., 2018; Pearce et al., 2012).

Apart from the significant deformation that is accommodated along the aforementioned structures, the Aegean plate undergoes internal deformation as well, indicated by numerous crustal faults with varied orientations and senses of slip. The region of NE Greece is dominated by roughly E-W trending, normal dip-slip faults within a tensional stress field which slightly switches from NNE-SSW to N-S as we move from the east (Thrace) to the west (eastern Macedonia). This N-S oriented tensional stress field continues further westwards across the Chalkidiki peninsula and central Macedonia. As a result, roughly E-W-striking, normal dip-slip faults occur, although NW-SE directions can be observed due to inherited structures from the previous (Pliocene—Early Pleistocene) NE-SW oriented tectonic extensional phase, which now are expected to have a more oblique movement (Lazos et al., 2022; Mercier et al., 1989; Pavlides & Kilias, 1987; Pavlides et al., 1990). In this part of northern Greece, earthquake activity is more intense compared to eastern Macedonia and Thrace, having both historical and instrumentally recorded significant earthquakes. Farther to the west on the northern Greek mainland, that is western Macedonia, the direction of the tensional stress field becomes NW-SE. A boundary from the previous region can be represented by the approximately NW-trending Axios Basin (AxB in Figure 1b). Western Macedonia is dominated by three major tectonic structures (i.e., Aliakmonas Fault Zone, and the Almopia and Ptolemais tectonic basins; see Caputo et al., 2012 and references therein), among which the most prominent is the NW-dipping Aliakmonas Fault Zone (AFZ in Figure 1b) where the 13 May 1995, M_w 6.5 Kozani earthquake occurred. Farther to the west, the core of the Pindos mountain-chain, that is the spine of the Greek mainland, lacks significant seismic activity in recent times, while few historical events (e.g., Papazachos & Papazachou, 2003) are too old to be accurately located. Our knowledge on active faulting in this area is also poor; an exception is the Konitsa fault, a rather small NW-dipping, normal fault associated with the moderate M_w 5.1 earthquake on 26 July 1996 (see Caputo et al., 2012 and references therein). Moving toward the Epirus coast, the stress field changes dramatically to compressional with a NE-SW direction. Affected by the AACZ, this compression has formed a fold-and-thrust belt with successive E-dipping thrusts. This belt is often cut and displaced by strike-slip faults, like the E-W trending Petoussi fault (PF in Figure 1b). This pattern is confined to the west by the AACZ and to the south by the CTFZ and the Amvrakikos Gulf graben (AG in Figure 1b). In this context, it is possible that the inner part of the Pindos mountain-chain represents a transition zone where the extension of western Macedonia gradually turns into compression. This is highlighted by the plunge decrease of the horizontal σ_1 axes, which end

Figure 1. (a) Regional tectonic setting of eastern Mediterranean. Black vectors show the sense of motion of tectonic plates relative to stable Eurasia according to Reilinger et al. (2006). (b) Seismotectonic framework of the Aegean region. Major structures and regional-scale faults are from the GreDaSS database (Caputo et al., 2012; Sboras, 2011), the DISS Working Group (2018) and Pérouse et al. (2017). Epicenters of earthquakes with $M_L \geq 4.0$ that occurred between 2008 and 2024 are illustrated as colored dots with respect to their hypocentral depth (taken from the earthquake catalog of the National Observatory of Athens at https://bbnet.gein.noa.gr/HL/databases/database). Focal mechanisms of earthquakes with $M_w \geq 5.5$ for the period 1997–2024 are taken from the European-Mediterranean Regional Centroid Moment Tensor (RCMT) Catalog (Pondrelli, 2002; https://rcmt2.bo.ingv.it/). NAF: North Anatolian Fault; NAT: North Aegean Trough; NAB: North Aegean Basin; SB: Skyros Basin; PiT: Pindos Thrust; AFZ: Aliakmonas Fault Zone; KFZ: Kaparelli Fault Zone; PF: Petoussi Fault; AACZ: Aegean-Apulian Collision Zone; CTFZ: Cephalonia Transform Fault Zone; KSF: Katouna-Stamna Fault Zone; AB: Almopia basin; PB: Ptolemais basin; TL: Trichonis lake; PG: Patras Gulf; GC: Gulf of Corinth; nEG: north Evia Gulf; sEG: south Evia Gulf; AG: Amvrakikos Gulf; MG: Maliakos Gulf; S: Sperchios; OS: Oraeoi Strait; AxB: Axios basin; sNAF: southern branch of the NAF.

21699356, 2026, 7, Downloaded from https://agupubs.onlinelibrary.wiley.com/doi/10.1029/2025JB033218, Wiley Online Library on [04/07/2026]. See the Terms and Conditions (https://onlinelibrary.wiley.com/terms-and-conditions) on Wiley Online Library for rules of use; OA articles are governed by the applicable Creative Commons License

21699356, 2026, 7, Downloaded from https://agupubs.onlinelibrary.wiley.com/doi/10.1029/2025JB033218, Wiley Online Library on [04/07/2026]. See the Terms and Conditions (https://onlinelibrary.wiley.com/terms-and-conditions) on Wiley Online Library for rules of use; OA articles are governed by the applicable Creative Commons License

up being horizontal west of Pindos Thrust (PiT in Figure 1b) compared to the almost vertical σ_1 axes to the east (Kapetanidis & Kassaras, 2019; Konstantinou et al., 2017).

In the Thessaly region of central mainland Greece, extension is oriented in a general N-S direction, with E-W normal faulting (Caputo & Pavlides, 1993). Understanding of the extension direction in northern Thessaly changed after the occurrence of two strong earthquakes on 3 March (M_w 6.3) and 4 March 2021 (M_w 6.0), given that contrary to the expected ca. E-W trending faulting, both shocks occurred on NW-SE-striking and NE-dipping faults, suggesting a NE-SW oriented extensional axis (Pavlides & Sboras, 2021; Sboras et al., 2022). Additionally, recent analysis of geodetic data revealed that the active tectonic strain rate field in this region is characterized by a NE-SW oriented extension (Chousianitis et al., 2024) which is consistent with the occurrence of the March 2001 normal faulting earthquakes.

South of the Thessaly region, the entire area which extends up to the Gulf of Corinth is characterized by strong extension (Chousianitis et al., 2013; Clarke et al., 1998; Hatzfeld et al., 1999). Its north margin is delineated by the approximately ESE-WNW-trending Sperchios River valley (S in Figure 1b), a tectonically controlled (half-) graben ending up in the Maliakos Gulf to the east (MG in Figure 1b). The prevailing, discontinuous, ESE-WNW trending, NNE-dipping normal faults along the southern margin of the Sperchios River valley (Eliet & Gawthorpe, 1995; Kilias et al., 2008; Whittaker & Walker, 2015) continue further to the ESE, merging with a ca. 100 km-long graben/rift, the North Evia Gulf (Roberts & Jackson, 1991), whose southern margin hosts a wide zone of well-developed, but segmented and discontinuous normal faults that strike parallel to the coastline. These faults cause subsidence along the coast and uplift of terraces inland (Cundy et al., 2010; Evelpidou et al., 2011; Goldsworthy & Jackson, 2001; Poulimenos & Doutsos, 1997; Pantosti et al., 2004; Papanastassiou et al., 2014; Roberts & Ganas, 2000; Roberts & Jackson, 1991). The North Evia Gulf together with the fault controlled Oraeoi Strait (OS in Figure 1b; Dewey & Şengör, 1979), separate northern Evia island from the extensional province of central Greece. This part of the island can be considered as a transitional zone in which the dominant shear of the two NAF branches in the Aegean Sea (i.e., NAT-NAB and Skyros Basin) gradually turns into extension toward the Greek mainland to the west. The transtensional regime acting in this part of the island is responsible for the occurrence of E-W and WNW-ESE-trending normal faults, along with NE-SW-trending oblique-slip faults with significant strike-slip component (Caroir et al., 2024; Palyvos et al., 2006), which are associated with large amounts of maximum shear strain rates (Chousianitis et al., 2024). Farther to the SE, the South Evia Gulf, which separates the southern part of Evia island from central Greece, represents another basin bounded along both sides by normal faults (Papanikolaou et al., 1988; Perissoratis & van Andel, 1991). This part of Evia is characterized by low seismic activity, although a seismic swarm in November-December 2022 with a maximum magnitude of M_w 4.8 according to the earthquake catalog of the National Observatory of Athens, revealed near strike-slip faulting principally on a NW-SE-striking nodal plane (Evangelidis & Fountoulakis, 2023).

West of the South Evia Gulf, Chousianitis et al. (2013) analyzed GPS velocities and suggested that the ~E-W striking Kaparelli fault zone (KFZ in Figure 1b) comprises a crustal block boundary separating the regions of Attica and Viotia. To the west, this boundary meets the Gulf of Corinth which is considered the most tectonically active structure in the Aegean and its formation started since approximately the Pliocene (e.g., Armijo et al., 1996; Keraudren & Sorel, 1987; Taylor et al., 2011). The Corinth Rift demonstrates a roughly N-S oriented rapid opening with westwards increasing rates from about 10 mm/yr at the eastern part to 14–16 mm/yr at the western part (e.g., Avallone et al., 2004; Briole et al., 2000; Chousianitis et al., 2013). There is some controversy about the tectonic setting of the Corinth Rift given that it is considered either an asymmetric (e.g., Goldsworthy & Jackson, 2001; Taylor et al., 2011) or a more symmetrical (e.g., Bell et al., 2008; Moretti et al., 2003) graben. Furthermore, a N-dipping, low-angle, detachment zone beneath northern Peloponnese associated with splay normal faulting has been proposed to control the opening of the rift, although its exact characteristics are also under some debate (Hatzfeld et al., 2000; Lambotte et al., 2014; Sorel, 2000; Rigo et al., 1996). To the WNW of the western part of the Corinth Rift, the western limit of the extensional province of central Greece occurs along the NNW-SSE-striking, left-lateral strike-slip Katouna-Stamna wrench fault zone (KSF in Figure 1b) which connects two E-W-trending extensional basins, the Amvrakikos Gulf to the north and the Trichonis Lake (TL in Figure 1b) to the south (Brooks et al., 1988; Clews, 1989; Le Pichon et al., 1995; Pérouse et al., 2017; Underhill, 1989). This fault zone has been identified as a tectonic block boundary (Chousianitis et al., 2015; Pérouse et al., 2017; Vassilakis et al., 2011), although it is unclear whether this boundary extends to the Patras Gulf (PG in Figure 1b; Pérouse et al., 2017) or it terminates to the western tip of the Corinth rift through the Trichonis Lake graben (Vassilakis et al., 2011). According to Pérouse et al. (2017), this 65 km-long fault zone is a recently formed, "immature" structure, probably inherited from the Alpine thrusts of the Hellenides orogenic belt.

South of the Gulf of Corinth, the Peloponnese exhibits diverse geodynamics. At its NW part, the large NE-SW oriented, blind right-lateral strike-slip fault where the 2,008 M_w 6.4 Andravida earthquake occurred, probably marks the boundary between the extension of the Gulf of Corinth and the contraction/shearing in the Ionian Sea. The eastern-central part of Peloponnese, which is less studied, demonstrates scattered recent seismicity, locally concentrated in small clusters; thus, no major active tectonic structure is yet known. Marine surveys (e.g., Papanikolaou et al., 1988; Piper & Perissoratis, 2003; van Andel et al., 1993) show that the eastern coastline is aligned with a large offshore fault depressing the seafloor. Toward the southeastern part of Peloponnese, seismic activity becomes slightly more intense with focal mechanisms of prevailing NNW-SSE-striking normal faulting in agreement with morphotectonic studies (e.g., Angelier et al., 1982; Fountoulis et al., 2014; Lyon-Caen et al., 1988; Papoulia & Makris, 2004; Papanastassiou et al., 2005). Similar geometry and kinematics persist in the southwestern part of Peloponnese where faults reveal an ENE-WSW oriented extensional strain field (e.g., Angelier et al., 1982; Armijo et al., 1992; Chousianitis et al., 2015; Le Pichon & Angelier, 1979; Lyon-Caen et al., 1988). The western coast is a rather complex area where normal dip-slip and strike-slip faulting occurs in two different striking directions: N-S and E-W, respectively (Fountoulis et al., 2014). Inland studies show that this neotectonic setting also shapes the morphological relief by forming horst and graben systems. In the deeper parts of the crust, the stress field changes to compression due to the occurrence of the western Hellenic subduction zone (e.g., Kassaras et al., 2016). Compression gradually rises up westwards, in the South Ionian Sea, until it finally prevails at all depths of the crust. The Ionian Sea is occupied by a wide fold-and-thrust belt consisting of imbricated thrusts and, occasionally, backthrusts which are all often cut and displaced by strike-slip faults (e.g., Haddad et al., 2020; Kokinou et al., 2005; Vassilakis et al., 2011; Wardell et al., 2014).

The south Aegean (i.e., from Cyclades islands and southwards) exhibits negligible internal deformation and behaves to a large degree as a rigid body, moving rapidly to the SSW with rates on the order of 34 mm/yr relative to Eurasia (Kahle et al., 2000; McClusky et al., 2000). Crete appears to be part of this rigid block, although onshore active faulting and seismicity imply some small amount of ongoing extensional deformation (e.g., Angelier et al., 1982; Caputo et al., 2010; Nicol et al., 2020). On the contrary, southeastern Aegean moves away from this block at about 10 mm/yr and therefore it is not attached to the rigid south Aegean (Kreemer & Chamot-Rooke, 2004; McClusky et al., 2000). The core of the south Aegean block is Cyclades which comprise a seismically quiet region. Seismic activity increases south of Amorgos island which is known for the 6 July 1956 M_S7.4 earthquake, whose aftershock distribution (Papadopoulos & Pavlides, 1992) and most focal mechanisms (Brüstle et al., 2014 and references therein) suggest the presence of a SE-dipping normal fault. Such a structure is in agreement with offshore surveys in the Amorgos Basin and seems to be part of a larger offshore NE-SW-striking fault system that reaches Santorini island (Hooft et al., 2017; Nomikou et al., 2018; Perissoratis & Papadopoulos, 1999; Tsampouraki-Kraounaki et al., 2021). In the eastern Aegean and western Anatolia, from the NAT until the oblique Hellenic subduction south of Rhodes, focal mechanisms' P- and T-axes indicate N-S extension and NE-SW shearing with locally formed transtension (e.g., Benetatos et al., 2004; Gessner et al., 2013; Hatzfeld et al., 1993; Sözbilir et al., 2011). In SW Turkey the deformation field is predominantly extensional, with only minor strike-slip on transfer segments. While some studies have proposed a left-lateral component along a prominent NE–SW structural trend linked to the trough system of the Hellenic subduction (Elitez et al., 2016; Özbakir et al., 2013), others argue that such strike-slip kinematics are difficult to reconcile with mapped faults, seismicity, and geodetic observations, indicating that extension accommodates most of the present-day deformation in the region (Howell et al., 2017; Nissen et al., 2022; Özkaptan et al., 2018).

3. Data Sets

3.1. GPS Velocity Field

The GPS-derived velocities we use are from the papers of Briole et al. (2021), Kurt et al. (2023) and Ergintav et al. (2022). These velocity solutions were derived using different processing approaches and are in different reference frames. Therefore, in order to ensure consistency, we aligned them into a common reference frame as part of the inversion process described in the next sections. In this context, by minimizing the velocities of the GPS sites located on the reference block (Eurasia), we estimated the angular velocities that rotate each velocity

21699356, 2026, 7, Downloaded from https://agupubs.onlinelibrary.wiley.com/doi/10.1029/2025JB033218, Wiley Online Library on [04/07/2026]. See the Terms and Conditions (https://onlinelibrary.wiley.com/terms-and-conditions) on Wiley Online Library for rules of use; OA articles are governed by the applicable Creative Commons License

field into a common Eurasian reference frame (Table S1 in Supporting Information S1). For velocity fields with no or very few sites on the reference frame block, the rotations are derived from alignment with the other blocks as described in McCaffrey (2005). This adjustment approach requires that sites of each velocity field are located on more than one block but does not require common sites. This workflow differs from others where GPS velocity fields are first rotated externally prior to block modeling. In our case, the reference frame alignment is treated as part of the inversion itself, with rigid rotations of individual velocity fields estimated simultaneously with block angular velocities and fault locking parameters, ensuring full kinematic consistency among all model components. The final GPS velocity field that we obtained includes 832 horizontal vectors in the Eurasian reference frame (Table S2 in Supporting Information S1), some of which are located in the interior of the (fixed) Eurasian plate. Sites on the Eurasian plate help constrain the rotations of the velocity fields.

3.2. Earthquake Slip Vectors

In addition to the GPS velocity data that densely cover the major part of continental Greece, we incorporated earthquake slip vectors in our inversions in order to bring additional constraints on block motions, especially on offshore block boundaries. Such data are particularly useful for blocks that are sparsely covered by GPS observations by improving their angular velocity estimations. From the European-Mediterranean Regional Centroid Moment Tensor (RCMT) Catalog (Pondrelli, 2002) we extracted 146 slip vector azimuths for earthquakes that are on block boundaries and are shallower than 40 km (Table S3 in Supporting Information S1). The choice of 40 km assures that we used only earthquakes located either on upper plate faults (for the entire study area) or on the subduction interface (for the southern part of the study area around the Hellenic Arc), which has been found to be seismogenic down to 40–50 km (Howell et al., 2017; Shaw & Jackson, 2010). We excluded earthquakes that likely occurred within the subducting lithosphere. The guide for the identification of such earthquakes was their P-axes, which are oriented parallel to the strike of the subduction zone revealing the along-arc contraction of the downgoing Nubian lithosphere (Benetatos et al., 2004; Shaw & Jackson, 2010; Taymaz et al., 1990). Since the slip vector directions were incorporated in the inversions to constrain the regional fault and block motions, we selected earthquakes that can be plausibly correlated with the structures that serve as block boundaries. From the two nodal planes of each focal mechanism, we selected as the fault plane the one that is consistent with the local neotectonic features and, hence, the associated boundary. During the inversions, we applied uncertainties of 10° to all earthquake slip vector azimuths (i.e., the azimuth of the horizontal component of the slip vector).

4. Features of the GPS Velocity Field

The resulting GPS velocity field of Section 3.1 used in the elastic block inversions includes the bulk of the Greek and western Anatolia GPS stations, combining the latest published data sets into a velocity solution in the Eurasian reference frame providing a dense coverage of the entire Aegean area. Using this GPS coverage, before developing the block model, we analyze a series of GPS velocity profiles to examine patterns and features of active deformation that will assist us in the delineation of block boundaries.

4.1. Microplate Slivers in North Aegean

The most striking feature in the south-to-north directed profile across the eastern Aegean (Figure 2a) is the prominent decrease in the profile-parallel and profile-normal velocities north of the northern branch of NAF. This feature demonstrates the result of the propagation of the NAF across the NAT and the NAB that disconnected the Aegean from Eurasia. A second notable feature in the along-profile direction is the step in the velocities between Lesvos and Chios islands. It is well-known that the northern and southern branches of the NAF enclose a crustal microplate sliver, as has been observed at other strike-slip boundaries around the world (i.e., California and New Zealand; Coffey et al., 2019; Little & Jones, 1998; Wallace et al., 2004). This observed difference in the along-profile velocity components between these two islands imply that an additional crustal microplate sliver, related to the northern sliver that is bounded by the NAF branches, exists in the north Aegean, separating Lesvos and Chios islands. This sliver, unlike the northern one whose kinematics are governed by shearing forces along strike-slip faults, exhibits combined strike-slip and extensional deformation, since ENE-WSW along with WNW-ESE normal faults delineate its southern boundary. This part of the eastern Aegeanwestern Anatolia demonstrates a quite complex structural regime involving significant NE-SW-striking shear, and roughly E-W-striking extensional faults (Chatzipetros et al., 2013; Sboras et al., 2021). The important role of the extensional structures in accommodating local strain in this area, which was manifested in 2007 with the M_w 6.3 Lesvos earthquake

21699356, 2026, 7, Downloaded from https://agupubs.onlinelibrary.wiley.com/doi/10.1029/2025JB033218, Wiley Online Library on [04/07/2026]. See the Terms and Conditions (https://onlinelibrary.wiley.com/terms-and-conditions) on Wiley Online Library for rules of use; OA articles are governed by the applicable Creative Commons License

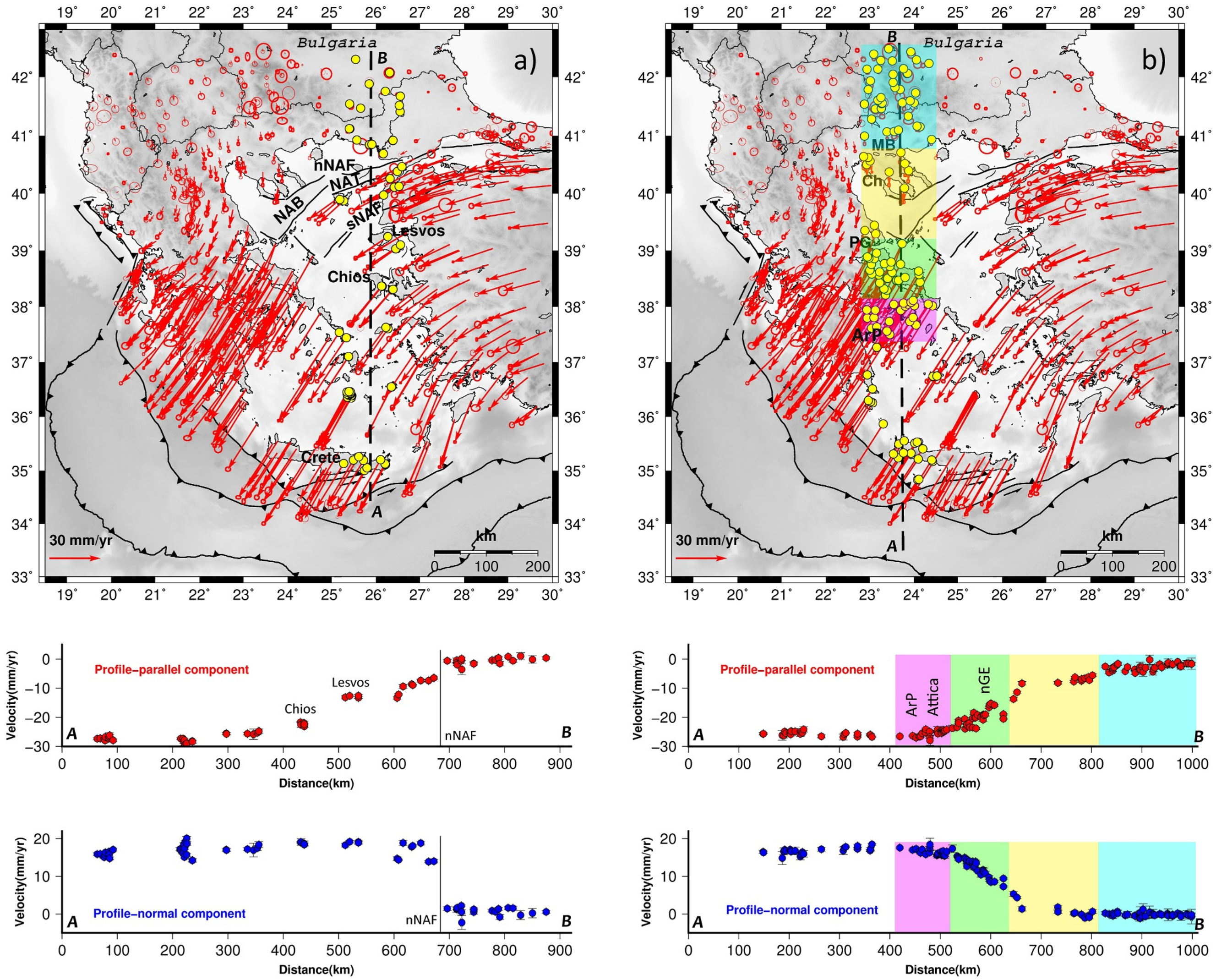

Figure 2. GPS velocity profiles across the (a) eastern and (b) central part of the Aegean region. The maps above the profile plots show horizontal GPS velocities with respect to Eurasia and 95 percent confidence ellipses. Dashed lines and yellow circles indicate location and GPS stations included in each profile, respectively. Plots with red data show profile-parallel velocities while plots with blue data show profile-normal velocities. Vertical line indicates the location where the northern branch of NAF (nNAF) crosses the eastern profile. NAF: North Anatolian Fault; NAT: North Aegean Trough; NAB: North Aegean Basin; MB: Mygdonia basin; Ch: Chalkidiki; PG: Pagasitikos Gulf; ArP: Argolis Peninsula; nGE: north Gulf of Evia.

(Chousianitis & Konca, 2018), is particularly evident in the profile of Figure 2a given that the velocity step is observed only in the along-profile direction. Farther south of Chios (roughly at km 350), the nearly uniform velocities of southern Aegean and Western Crete stations in the along- and cross-profile directions point to a transition into an area of little present-day internal deformation.

4.2. Segmented Extension From Western Bulgaria to NE Peloponnese

In the along-profile direction of the profile shown in Figure 2b, five gradients of velocity can be distinguished. Starting in the north, a smooth gradient is observed in the western Bulgaria-central Macedonia region extending up to the Mygdonia basin. Palaeoseismological studies on particular faults in central Macedonia and the Mygdonia Basin documented slip-rates between 0.1 and 0.3 mm/yr (Papanikolaou et al., 2022). Moving southwards, the faster increase of the south oriented velocities throughout Chalkidiki peninsula reveals a stronger N-S extension that can be traced until the E-W-trending normal faults of Pagasitikos Gulf. Farther south, the most pronounced gradient of velocity in the along-profile direction, can be attributed to the transtensional graben system of north Gulf of Evia. Transtension there is taken up by the coastal fault systems of north Evia and central

21699356, 2026, 7, Downloaded from https://agupubs.onlinelibrary.wiley.com/doi/10.1029/2025JB033218, Wiley Online Library on [04/07/2026]. See the Terms and Conditions (https://onlinelibrary.wiley.com/terms-and-conditions) on Wiley Online Library for rules of use; OA articles are governed by the applicable Creative Commons License

mainland Greece which include the Maliakos/Arkitsa and Atalanti faults (Chousianitis et al., 2013; Sboras et al., 2025). From the palaeoseismologically estimated 0.4–1.6 mm/yr throw rate for the Atalanti fault by Pantosti et al. (2004), we can estimate a slip rate of 0.57–2.49 mm/yr assuming a 40°–45° dipping fault plane. This transtensional deformation, which is result of the wide shear zone that dominates the North Aegean Sea (Sboras et al., 2025), extends up to the Kaparelli–Erithres faults where a transition to a smoother velocity gradient across Attica and Argolis Peninsula in NE Peloponnese is evident. This domain of decreased extensional rates marks the termination of a large zone of N-S directed extension that spreads for approximately 500 km, from western Bulgaria to NE Peloponnese. The profile-normal velocity components highlight that this extension is primarily N-S directed from western Bulgaria to Chalkidiki peninsula, as seen by the flat profile-normal velocities, while further south their gradual increase up to NE Peloponnese points to a change in the extension direction toward the NNE-SSW.

4.3. Three Individual Domains in Central Ionian Sea

The profile across the central Ionian Sea islands (Figure 3) primarily demonstrates that (a) Strofades (where STRF station is located) move independently of Zakynthos and (b) Zakynthos moves independently of Cephalonia and Lefkada. This suggests the existence of three different domains and highlights the complexity of deformation in this relatively confined region where the northwestern end of the active Hellenic subduction front meets an area where the bulk of interseismic geodetic strain is completely released seismically at NE-SW strike-slip faults among which the most notable is the CTFZ. Furthermore, the profile-parallel velocity components of Lefkada stations highlight the persistence of onshore contraction associated with a considerable amount of strain accumulation (Chousianitis et al., 2015; Ganas et al., 2013). Finally, onshore Cephalonia, the two stations which are located at Paliki Peninsula (KIPO and KEFA) deviate from the other stations on the island in the along-profile direction. Although we acknowledge that the velocity gradient of the southern Cephalonia stations, whose orientation is perpendicular to the CTFZ, mimic the pattern of interseismic elastic deformation (Savage & Burford, 1973), this velocity deviation could imply different kinematic behavior of Paliki Peninsula compared to the rest of the island. The boundary that differentiates Paliki Peninsula could be related to the active NNE-SSW faults which are located at the eastern side of Paliki Peninsula and were activated during the 2014 earthquake sequence (Briole et al., 2015; Merryman Boncori et al., 2015). This pattern of segmented kinematics agrees with Shaw and Jackson (2010), who emphasize along-strike variability near the western termination of the Hellenic subduction system.

4.4. Influence of Apulia Collision in Western Greece and the Boundary of Axios Basin

The profile of Figure 4 is oriented normal to the collision zone of the Apulian platform with Eurasia in NW Greece as well as to the strike of the Pindos Thrust. In the cross-profile direction we observe a sign reversal in the velocities along an axis that connects stations GARD and DERV and which coincides with the east dipping Paramythia thrust. This change in the direction of the GPS velocities is associated with the collision of Apulia with Eurasia and highlights that its impact is confined within a zone that extents west of Paramythia thrust. This is further corroborated by the contraction rates, as the boundary separating shortening from extension also separates stations exhibiting opposite signs in the profile-normal velocities (Figure 4). East of the Paramythia thrust, the profile-normal velocity components smoothly increase until the Axios Basin, where an evident reversal toward lower values takes place (expressed through the switch of the sign of slope). These two opposite gradients of velocity in the profile correlate well with the change of the extension direction, which rotates from NW-SE to N-S at the territory of Axios Basin. In this context, the domain to the west of Axios Basin constitutes a region with NE-SW trending normal faults, as a result of a NW-SE oriented extension, among which the most prominent is the NW-dipping Aliakmonas Fault Zone, some segments of which ruptured during the M_w 6.5 earthquake in 1995 (e.g., Caputo et al., 2012; Sboras, 2011). East of Axios Basin, the direction of extension becomes N-S and is mostly taken up by E-W trending normal faults (e.g., Caputo et al., 2012; Sboras, 2011).

4.5. Quantification of the Effect of Apulian Collision on Upper Plate Deformation

To highlight additional features of the GPS velocity field that are not apparent in the Eurasia-fixed reference frame, we expressed the GPS velocities relative to central Aegean. We derived this Aegean-fixed reference frame by minimizing, in a least squares sense, the velocities of the GPS sites circled in blue in Figure S1 of Supporting Information S1. The GPS velocity field with respect to fixed central Aegean is tabulated in Table S1 in Supporting

21699356, 2026, 7, Downloaded from https://agupubs.onlinelibrary.wiley.com/doi/10.1029/2025JB033218, Wiley Online Library on [04/07/2026]. See the Terms and Conditions (https://onlinelibrary.wiley.com/terms-and-conditions) on Wiley Online Library for rules of use; OA articles are governed by the applicable Creative Commons License

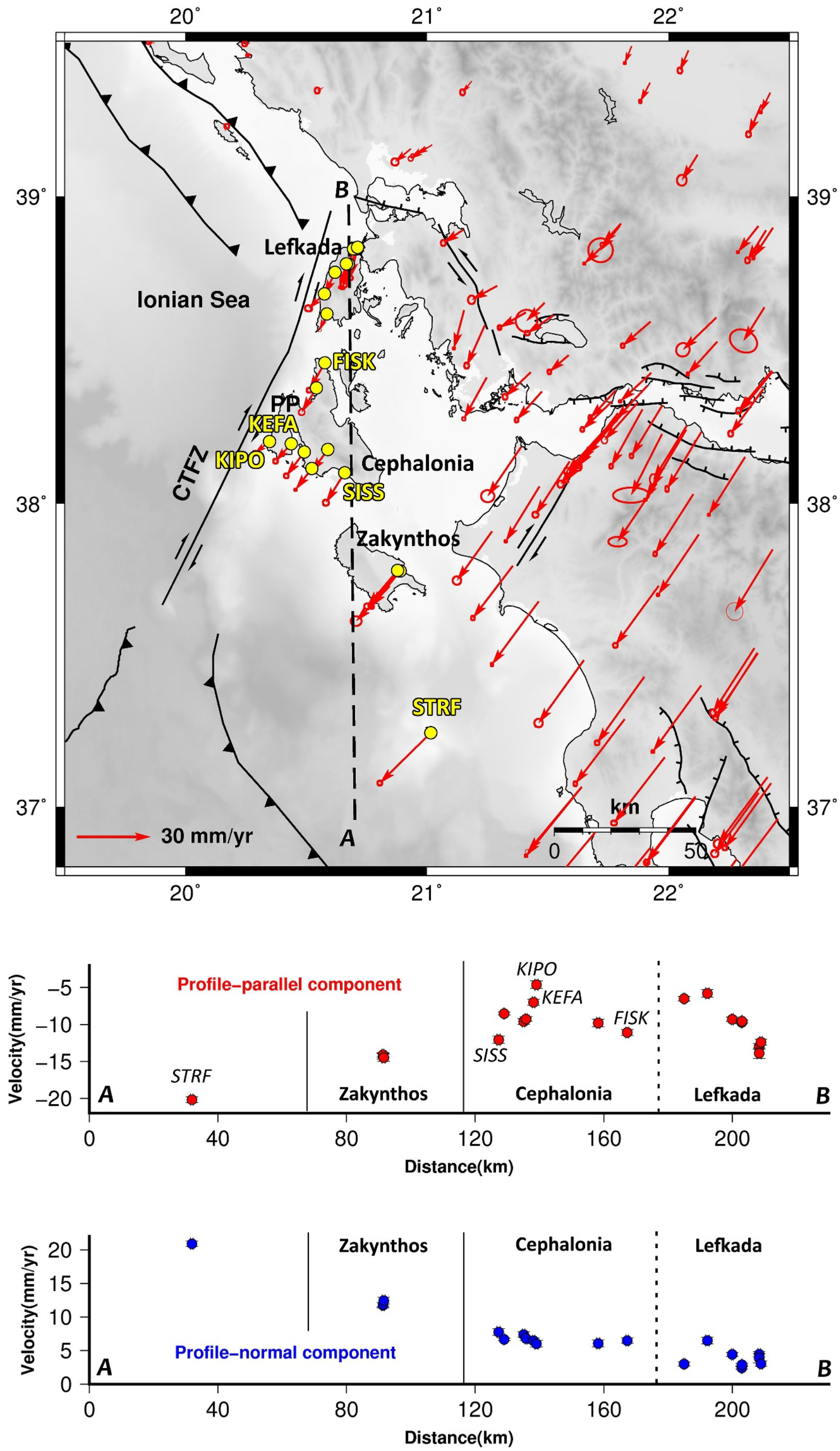

Figure 3. GPS velocity profile across the central Ionian Sea. (top) Map showing horizontal GPS velocities with respect to Eurasia and 95 percent confidence ellipses. Dashed line and yellow circles indicate location and GPS stations included in the profile, respectively. (bottom) Upper plots with red data show profile-parallel velocities while lower plots with blue data show profile-normal velocities. Annotations (station names and toponyms) match up with those in the map. Vertical lines delimit GPS stations located on each of the four central Ionian Sea islands discussed in text. CTFZ: Cephalonia Transform Fault Zone; PP: Paliki Peninsula.

21699356, 2026, 7, Downloaded from https://agupubs.onlinelibrary.wiley.com/doi/10.1029/2025JB033218, Wiley Online Library on [04/07/2026]. See the Terms and Conditions (https://onlinelibrary.wiley.com/terms-and-conditions) on Wiley Online Library for rules of use; OA articles are governed by the applicable Creative Commons License

10.1029/2025JB033218

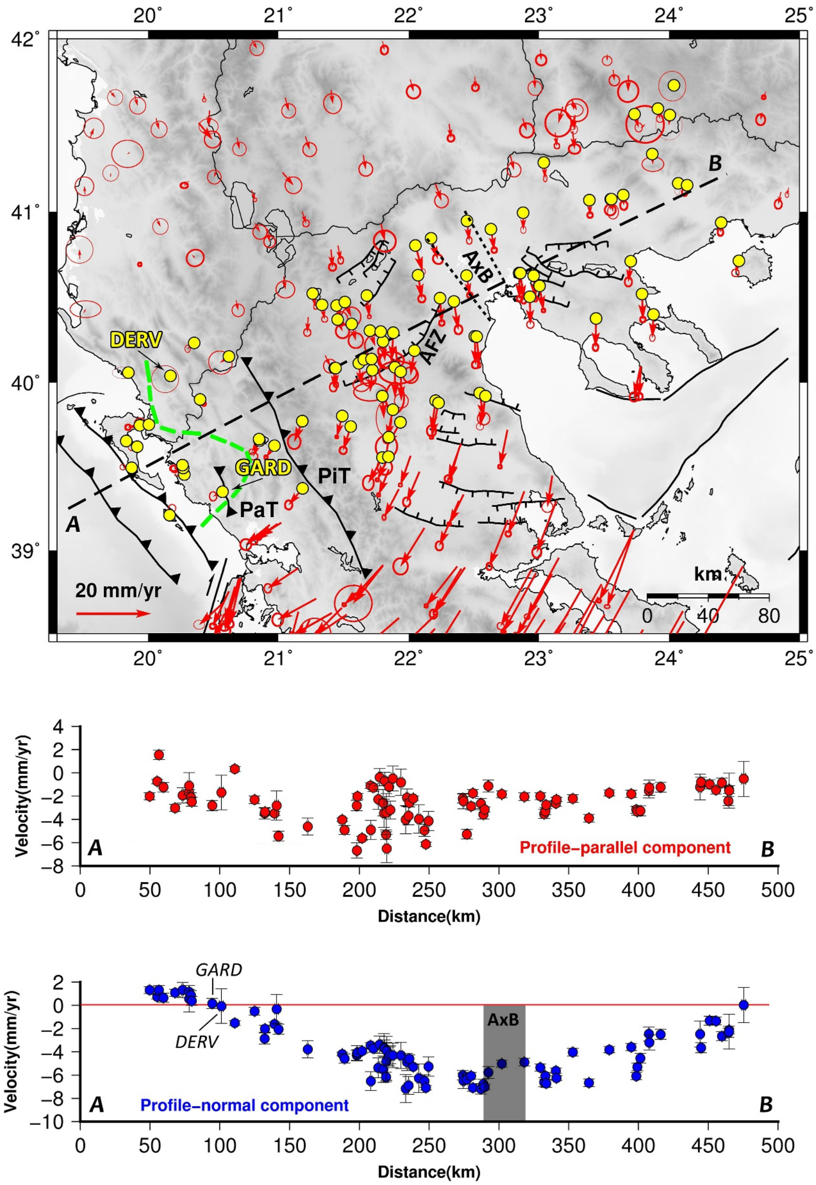

Figure 4. GPS velocity profile across NW and *n* Greece. (top) Map showing horizontal GPS velocities with respect to Eurasia and 95 percent confidence ellipses. Dashed line and yellow circles indicate location and GPS stations included in the profile, respectively. (bottom) Upper plots with red data show profile-parallel velocities while lower plots with blue data show profile-normal velocities. Green dashed line represents the transition between shortening and extension from the dilatation rates of Chousianitis et al. (2024). Gray area annotated as AxB in the profile-normal plot corresponds to the Axios Basin as discussed in text. Its location is also delineated by the two dotted lines in the map. Red horizontal line in the profile-normal plot corresponds to zero velocity value. Stations whose names are shown with yellow in the map, have been also annotated in the profile-normal velocity plot. PiT: Pindos Thrust; PaT: Paramythia Thrust; AxB: Axios Basin; AFZ: Aliakmonas Fault Zone.

Information S1. In this reference frame the velocities of stations located at northern Ionian Sea-Epirus are oriented approximately perpendicular to the Apulian collision front (Figure 5). A velocity profile parallel to the direction of the vectors allows us to assess the crustal shortening induced by the movement of the Apulian platform toward continental NW Greece. The effect of the Apulian collision on upper plate deformation, as defined by the profile shown in Figure 4, is confined up to the Paramythia thrust (a few kilometers east of station GARD). Considering that the profile-parallel velocity components drop off from 34 mm/yr to 30 mm/yr over about 40 km from Paxoi islands (where station PAXO is located) to stations IGOU-GARD, we estimate a contraction on the order of

21699356, 2026, 7, Downloaded from https://agupubs.onlinelibrary.wiley.com/doi/10.1029/2025JB033218, Wiley Online Library on [04/07/2026]. See the Terms and Conditions (https://onlinelibrary.wiley.com/terms-and-conditions) on Wiley Online Library for rules of use; OA articles are governed by the applicable Creative Commons License

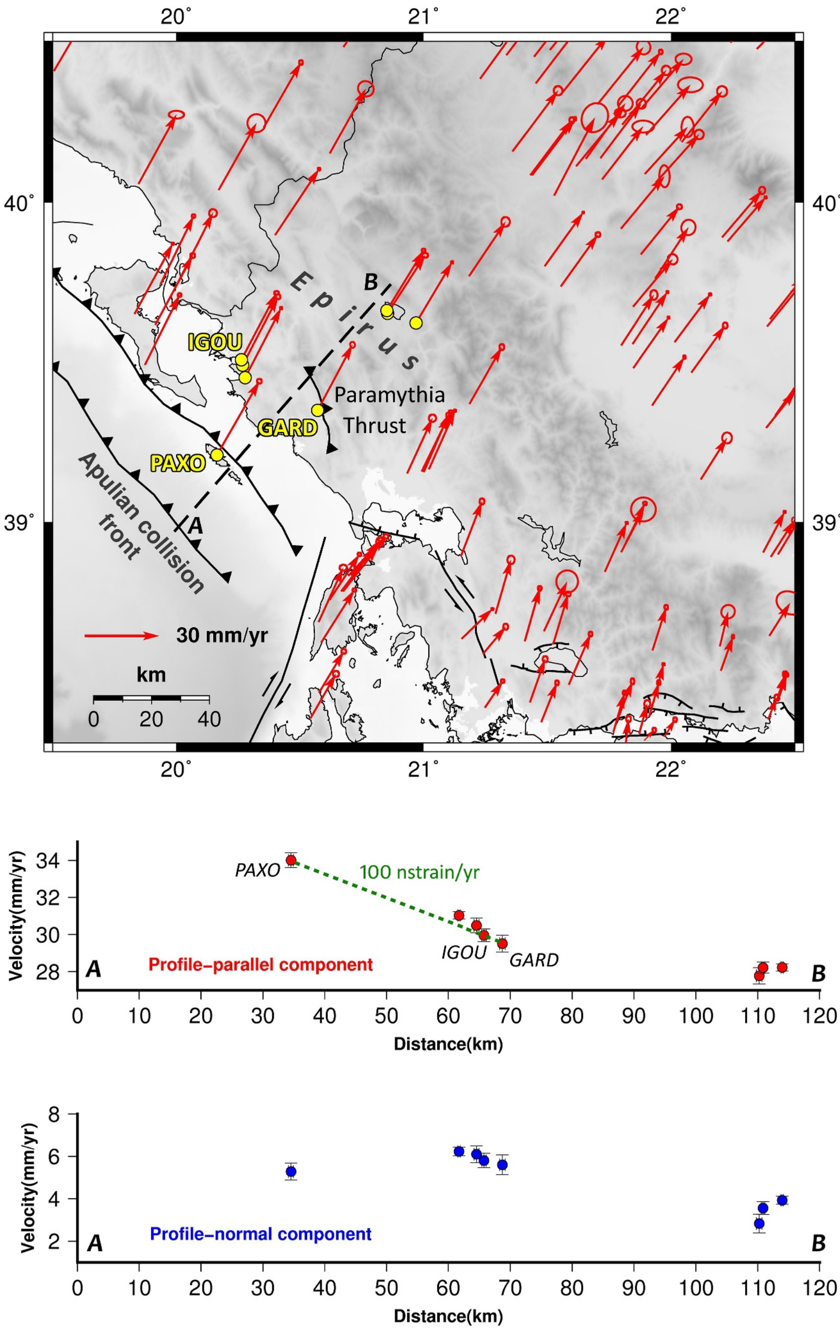

Figure 5. GPS velocity profile in the region where the Apulian platform collides with NW Greece. (top) Map showing horizontal GPS velocities with respect to central Aegean and 95 percent confidence ellipses. Dashed line and yellow circles indicate location and GPS stations included in the profile, respectively. (bottom) Upper plots with red data show profile-parallel velocities while lower plots with blue data show profile-normal velocities. Green dashed line corresponds to the 100 nstrain/yr contraction measured between stations PAXO and GARD. Stations whose names are shown with yellow color in the map, have been also annotated in the profile-parallel velocity plot.

100 ns/yr. Since little seismic activity occurs offshore and near the coast of Epirus, this significant amount of strain is taken up by a few nearby onshore reverse faults of the fold-and-thrust compressional belt. Unfortunately, no geological or palaeoseismological studies are available for estimating slip rates on any of the thrusts within this belt.

21699356, 2026, 7, Downloaded from https://agupubs.onlinelibrary.wiley.com/doi/10.1029/2025JB033218, Wiley Online Library on [04/07/2026]. See the Terms and Conditions (https://onlinelibrary.wiley.com/terms-and-conditions) on Wiley Online Library for rules of use; OA articles are governed by the applicable Creative Commons License

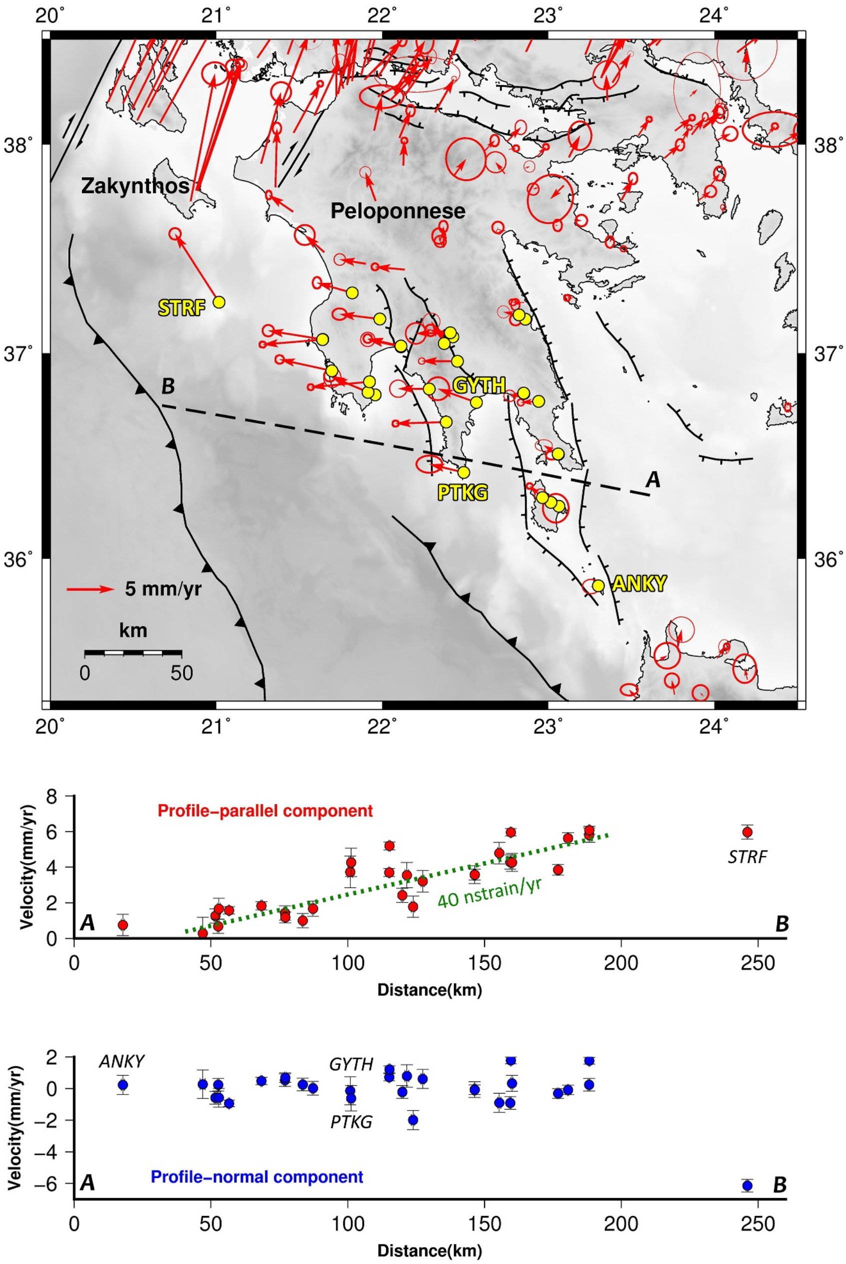

Figure 6. GPS velocity profile across southern Peloponnese. (top) Map showing horizontal GPS velocities with respect to central Aegean and 95 percent confidence ellipses. Dashed line and yellow circles indicate location and GPS stations included in the profile, respectively. (bottom) Upper plots with red data show profile-parallel velocities while lower plots with blue data show profile-normal velocities. Green dashed line corresponds to extension of 40 nstrain/yr due to the westward increasing velocities. Stations whose names are shown with yellow in the map, have been also annotated in the profile-parallel velocity plot.

4.6. E-W Extension at Southern Peloponnese

In the central Aegean reference frame, GPS sites in south Peloponnese show a systematic westward motion which increases toward the west (Figure 6). A WNW-ESE directed velocity profile shows a relative motion on the order of 6 mm/yr across ~150 km, corresponding to a crustal extension of 40 ns/yr, that is in general parallel to the T-axes of normal faulting earthquakes that have occurred across this part of Peloponnese (Benetatos et al., 2004; Kiratzi & Louvari, 2003). However, the larger fraction of this crustal extension occurs to the west of the line connecting stations PTKG and GYTH, where the deformation rate is, at least, twice the rate that occurs across the

21699356, 2026, 7, Downloaded from https://agupubs.onlinelibrary.wiley.com/doi/10.1029/2025JB033218, Wiley Online Library on [04/07/2026]. See the Terms and Conditions (https://onlinelibrary.wiley.com/terms-and-conditions) on Wiley Online Library for rules of use; OA articles are governed by the applicable Creative Commons License

eastern leg of Peloponnese. In this context, it is plausible to distinguish two zones, located on either side of the aforementioned line, that accommodate the west directed extension of south Peloponnese. Overall, this pattern suggests that the deformation is likely accommodated by a mixture of distributed strain (mostly across SW Peloponnese) and localized fault slip, although quantifying their relative contributions will require denser geodetic data. As regards the kinematic behavior of Peloponnese, from its central part and northwards, the velocity vectors change their direction and the westward motion vanishes, highlighting a largely different kinematic behavior of the southern part compared to the rest of Peloponnese which is reflected at the direction change of the principal horizontal strain rate axes (Chousianitis et al., 2015). Finally, it is evident that the profile-parallel and profile-normal velocity components of STRF station (located on Strofades islands) are largely different from those of stations located in Peloponnese. This implies that Strofades islands are disconnected from Peloponnese, in addition to Zakynthos (evident in the profile of Figure 3), most likely belonging to an independent domain.

4.7. Low Level of Deformation Onshore Crete

Crete is part of a complex, multi-directional faulting regime that characterizes the southern Aegean. It demonstrates E-W, N-S and NNE-SSW oriented normal faults (e.g., Caputo et al., 2010; Nicol et al., 2020; Veliz et al., 2018); however, slip rate estimates are available for only a few faults in eastern Crete which have been derived from displaced marine terraces or cosmogenic ^{36}Cl dating and indicate relatively low rates, ranging between 0.2 and 1.1 mm/yr (Gaki-Papanastassiou et al., 2009; Mechernich et al., 2023). A GPS velocity profile across Crete suggests that the island undergoes little internal deformation (Figure 7). Only a small component of arc-parallel extension is visible that amounts to 6 nstrain/yr (relative motion of 1.5 mm/yr across ∼250 km) that is possibly taken up by N-S normal faults that have been mapped across Crete. Also, although the along- and cross-profile directions demonstrate minor crustal deformation, a sign reversal of the profile-normal velocity components is observed eastwards of stations MURT and RETH resulting in a differential motion of the island in the north-south direction. This behavior may reflect differential locking along the Hellenic subduction system, as discussed in our companion paper (Chousianitis et al., 2026).

5. Kinematic Block Modeling

5.1. Block Model Set-Up

To better understand the crustal deformation pattern across the Aegean region, we adopted the elastic block modeling approach of McCaffrey (2002) and built a 3D kinematic model that consists of a number of closed polygons. The sides of these polygons can be either boundaries which are capable of inducing elastic deformation around them or free-slipping segments that do not produce any elastic strain. Previous block modeling studies in the Aegean and western Turkey have also attempted to interpret the observed deformation field in terms of relative motions between kinematically distinct crustal blocks (Nyst & Thatcher, 2004; Reilinger et al., 2006; Tiryakioğlu et al., 2013; Vernant et al., 2014). The block boundaries of our model were defined on the basis of the locations of major known active faults (discussed in Section 2 and illustrated in Figure S2 of Supporting Information S1), the seismicity distribution (Figure 1) and evidence for the presence of narrow active zones which imply non-continuum deformation processes that were seen in the GPS velocity profiles (discussed in Section 4). Apart from the free-slip boundaries of our model, boundaries where we adjust fault locking in the inversions represent real world active structures. Given that so far little is known of the slip rates and the degree of locking on the majority of them, we use our model to provide new knowledge on the interseismic behavior of the main active structures of mainland Greece and the Aegean. The block boundaries typically coincide with a single main structure, though in some cases they have been drawn to coarsely approximate a more complex diffuse zone of faulting such as the boundary that outlines the Gulf of Corinth. In this latter case, what is estimated through the block modeling approach is the total slip rate across that zone. The kinematic character of block boundaries is not prescribed a priori, but is determined by the inversion through the estimated relative block rotations. Figure S2 in Supporting Information S1 depicts the constructed block model and Table S4 in Supporting Information S1 summarizes the complete list of parameters for all block-bounding faults, including their dip angles and dip directions that were primarily taken from the GreDaSS database (Caputo et al., 2012; Sboras, 2011). We note that the block model illustrated in Figure S2 in Supporting Information S1 exhibits the maximum model complexity and it is not the preferred model which we determined after testing several different configurations where some of the depicted blocks in Figure S2 in Supporting Information S1 were merged. More details about these runs with the alternative configurations are given in Section 5.2. As regards the Aegean subduction interface, we used the

21699356, 2026, 7, Downloaded from https://agupubs.onlinelibrary.wiley.com/doi/10.1029/2025JB033218, Wiley Online Library on [04/07/2026]. See the Terms and Conditions (https://onlinelibrary.wiley.com/terms-and-conditions) on Wiley Online Library for rules of use; OA articles are governed by the applicable Creative Commons License

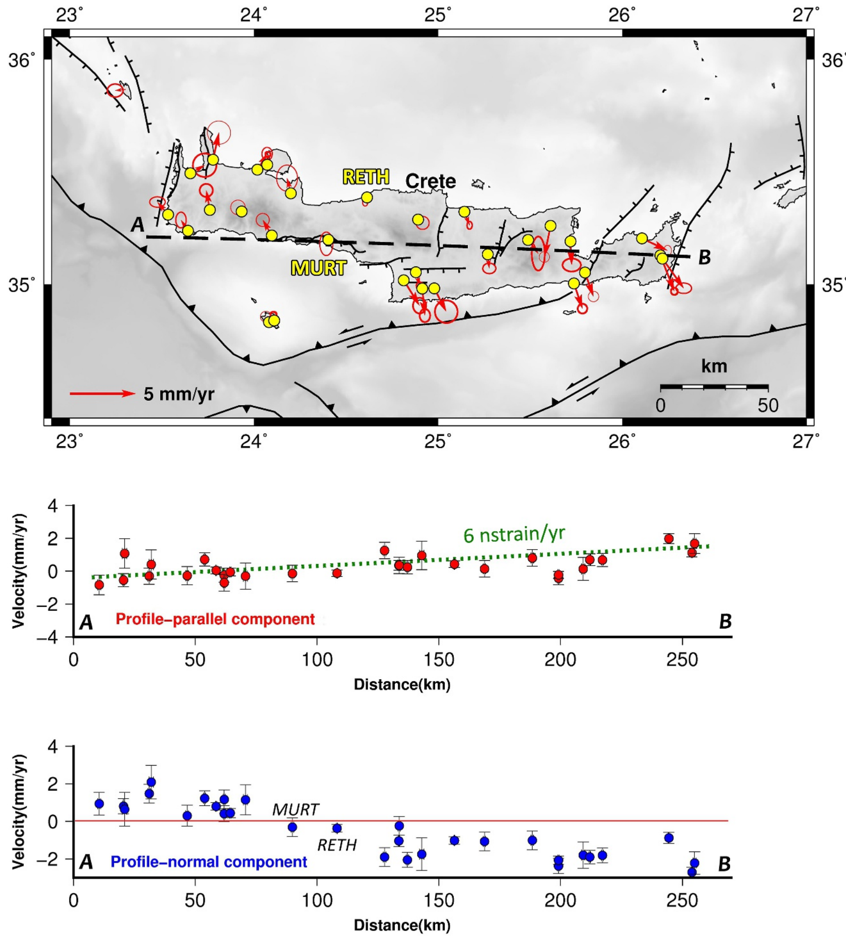

Figure 7. GPS velocity profile across Crete. (top) Map showing horizontal GPS velocities with respect to central Aegean and 95 percent confidence ellipses. Dashed line and yellow circles indicate location and GPS stations included in the profile, respectively. (bottom) Upper plots with red data show profile-parallel velocities while lower plots with blue data show profile-normal velocities. Green dashed line corresponds to ∼E-W extension of 6 nstrain/yr onshore Crete. Red horizontal line in the profile-normal plot corresponds to zero velocity value. Stations whose names are shown with yellow in the map, have been also annotated in the profile-parallel velocity plot.

geometry of the subducting slab defined by Bocchini et al. (2018). In our modeling, apart from the crustal blocks that cover the broader Aegean region, we defined three major plates, that is, the Nubian, Eurasian and Anatolian plates whose geometry was taken from Bird (2003).

5.2. Elastic Modeling Approach and Best Fit Model

In order to interpret the present-day active deformation field of the Aegean region we invert the GPS velocities (Figure S3a in Supporting Information S1) and the earthquake-derived slip vector azimuths (Figure S3b in Supporting Information S1) using the TDEFNODE code (McCaffrey, 2009). The GPS velocities incorporate the combined effects of instantaneous rigid body rotations and interseismic elastic strain along the block-bounding faults. The latter represents the influence of active faults on the GPS velocity field and occurs due to along-fault frictional forces that prevent the steady slip of these faults with their long-term rates, giving rise to an amount of slip rate deficit. The effect of this process is a decrease of velocities close to a locked fault because the respective GPS sites cannot move with their rates estimated from the rotations. The slip rate deficit can be quantified through the scalar coupling coefficient φ whose minimum ($\varphi = 0$) and maximum ($\varphi = 1$) values indicate full creep and complete fault locking, respectively (McCaffrey, 2002). The model parameters which we will estimate through the TDEFNODE inversions include angular velocities for the rotation of the GPS velocity fields into the Eurasian reference frame, angular velocities of tectonic blocks, and coupling coefficients at the

21699356, 2026, 7, Downloaded from https://agupubs.onlinelibrary.wiley.com/doi/10.1029/2025JB033218, Wiley Online Library on [04/07/2026]. See the Terms and Conditions (https://onlinelibrary.wiley.com/terms-and-conditions) on Wiley Online Library for rules of use; OA articles are governed by the applicable Creative Commons License

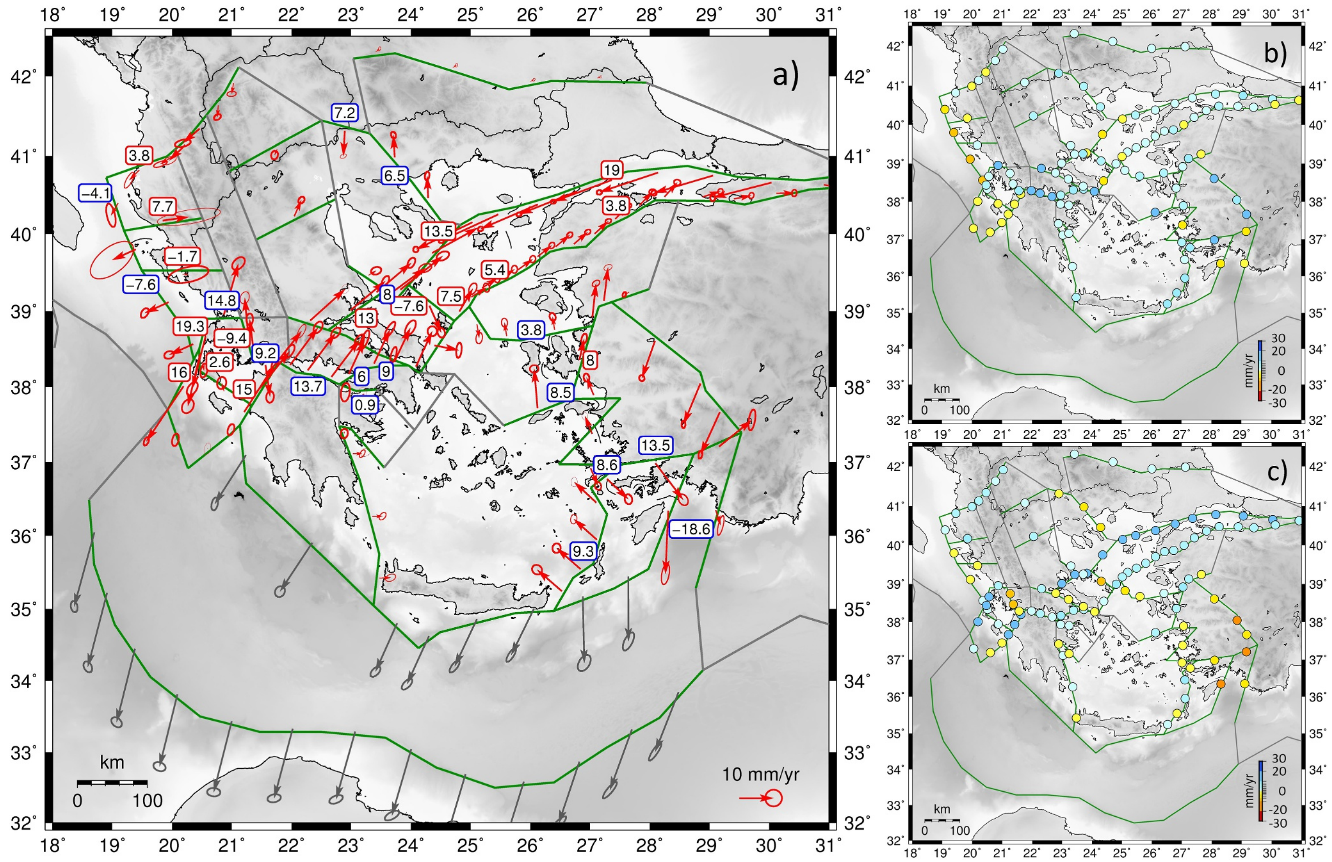

Figure 8. (a) Predicted relative slip vectors across the boundaries of the best fit block model with their 95% confidence ellipses. They depict the movement of the hanging wall relative to the footwall (tail of vector originates on moving block). Vectors in gray refer to structures of the Hellenic subduction system which are discussed in the companion article (Chousianitis et al., 2026). Numbers in boxes correspond to rates mentioned in the text, with red-outlined boxes denoting strike-slip motion (dextral positive) and blue-outlined boxes denoting dip-slip motion (extension positive). (b) Fault-normal and (c) fault-parallel components of the relative slip vectors. Positive values indicate divergence and right-lateral shear. Green and gray lines of the block model represent real world active faults where locking was applied and free-slip boundaries, respectively.

nodes that outline the 3-D geometry of the block-bounding faults. At each of the fault nodes, a long-term slip vector is estimated from the block angular velocities together with a scalar coupling value. The associated contribution to the surface deformation that stems from the elastic slip rate deficit is estimated using the half-space dislocation equations of Okada (1992) while applying the backslip concept at each individual patch along the fault surface. TDEFNODE employs iterative nonlinear inversions of all input data to simultaneously estimate the model parameters. In particular, it applies grid search and simulated annealing to find a set of parameters that minimizes the data misfit function which is defined as the sum of penalties associated with parameter constraints plus the reduced chi-square statistic X_n^2 (i.e., the chi-square per degrees of freedom): $F = (R^T \mathrm{W} R)/\mathrm{dof}$, where R is the matrix of the data residuals, W is the weight matrix, and dof is the degrees of freedom which equals the number of observations minus the number of fitted parameters.

After defining the tectonic blocks of the Aegean region illustrated in Figure S2 of Supporting Information S1, we ran several inversions to test a variety of models in an effort to find a preferred configuration that matches the GPS and earthquake slip vector data. To this end, we started from a simple four-block model resembling the one used by Nyst and Thatcher (2004), and by dividing larger blocks to smaller ones, we gradually increased model complexity. Each new run was assessed on the basis of its reduced chi-square misfit, the weighted variance of data, and when necessary by using an F test. More specifically, in order to accept an updated block model configuration, we checked that we achieved a lower data misfit compared to the previous model which implies a better fit to the observations, and that the variance was reduced, as it should be any time we add parameters. Finally, when these two conditions were satisfied, an F test was performed to check whether or not the addition of

21699356, 2026, 7, Downloaded from https://agupubs.onlinelibrary.wiley.com/doi/10.1029/2025JB033218, Wiley Online Library on [04/07/2026]. See the Terms and Conditions (https://onlinelibrary.wiley.com/terms-and-conditions) on Wiley Online Library for rules of use; OA articles are governed by the applicable Creative Commons License

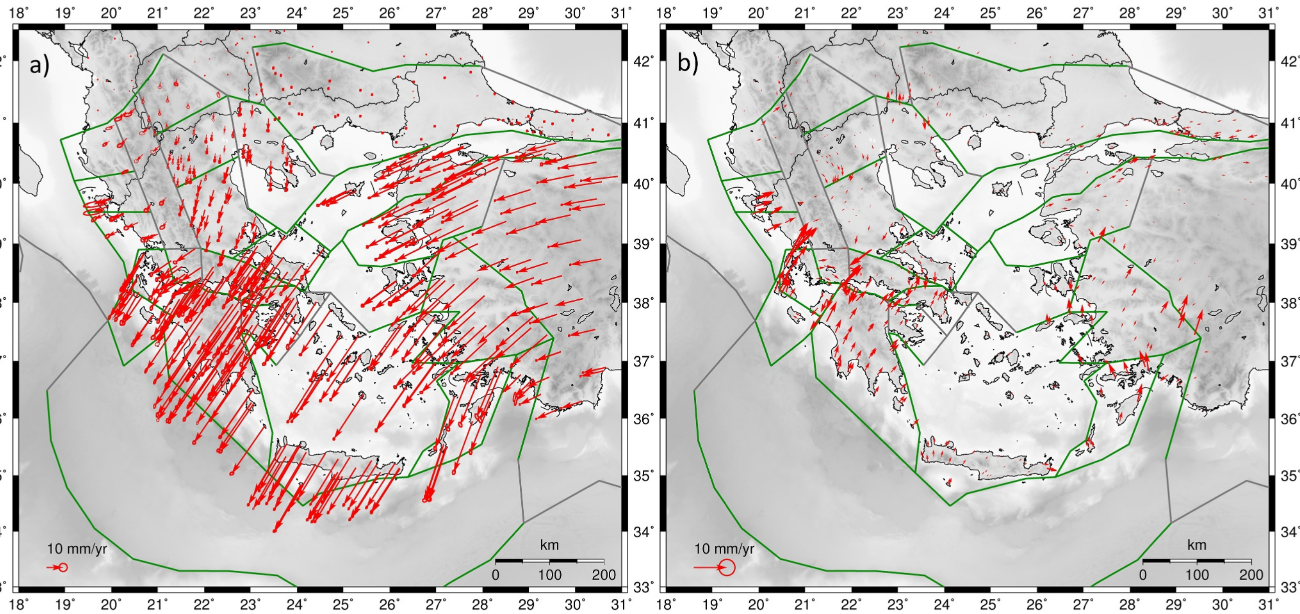

Figure 9. (a) Rotational component of the GPS velocity field attributable to block rotations. (b) Elastic component of the GPS velocity field attributable to interseismic locking on active faults.

the new blocks was statistically warranted. In this way, after evaluating which faults and tectonic blocks are the more important in reproducing our data, we determined the model shown in Figure S4 of Supporting Information S1 and Figure 8 as the preferred model. Details about the other nine models that we tested are included in Text S1 and Figures S6–S15 of the Supporting Information S1.

In our best fit model we obtained a $X_n^2 = 4.865$ and estimated 142 free parameters using 832 GPS velocities (1664 observations) and 146 earthquake slip vector azimuths. The residual GPS velocities, which do not exhibit notable systematic orientations, are shown in Figure S4 in Supporting Information S1 and reported in Table S2 of Supporting Information S1, while the fits to the earthquake slip vectors are reported in Table S3 of Supporting Information S1. The free parameters that we adjusted in the inversion consist of 3 angular velocity parameters for each of the 3 GPS velocity fields and the 26 blocks, and 1 coupling coefficient for each of the 519 fault nodes. The X_n^2 for the GPS data set equals to 4.208, while the corresponding normalized root mean square (nrms) and weighted root mean square (wrms) are 1.892 and 1.407 mm/yr, respectively. Similarly, the X_n^2 for the slip vectors is 8.029, the nrms is 2.034 and the wrms is 28.336°. As regards the individual tectonic blocks of the best fit model, the wrms values range from 0.355 to 3.71 mm/yr. The lowest wrms misfit was obtained for the Nubian plate, where 82 GPS observations were used to constrain its rotation relative to Eurasia. Figure S5 in Supporting Information S1 shows the position of the new Nubia-Eurasia Euler pole in conjunction with previously published estimates.

An inversion in which we solved for block rotations only and disregarded locking on crustal faults gave a poor fit to the data ($X_n^2 = 8.214$, 1733 degrees of freedom). This result implies that the GPS velocities in the Aegean region include a significant short-term elastic component due to locking on active faults. Accordingly, any attempt to interpret the deformation only on the basis of rotations of completely rigid tectonic blocks, without taking into account the strain accumulation along their boundaries due to locking, will fail to account for the role of the fault-induced elastic strain that appears to have important influence on the GPS velocity fields that span the Aegean region. An inversion in which we maximized the elastic deformation component by assigning full uniform coupling to all faults of the model ($X_n^2 = 14.427$, 1733 degrees of freedom), produced a larger misfit compared to the best fit model, indicating that the optimum approach is to solve for the coupling coefficients. Therefore, it is essential to consider both the rotational and the elastic component of the GPS velocity field when kinematic models are invoked to investigate the active tectonics of the Aegean region. The contribution of these two components to the velocity field predicted by our best fit model is illustrated in Figure 9. We note that in all of the inversions presented in this paper, we estimated a uniform coupling coefficient value φ for each fault.

21699356, 2026, 7, Downloaded from https://agupubs.onlinelibrary.wiley.com/doi/10.1029/2025JB033218, Wiley Online Library on [04/07/2026]. See the Terms and Conditions (https://onlinelibrary.wiley.com/terms-and-conditions) on Wiley Online Library for rules of use; OA articles are governed by the applicable Creative Commons License

Attempts where we allowed spatial variations in coupling, either along strike, or downdip with the constraint of a monotonic decrease of φ with depth, resulted in solutions with larger X_n^2 and larger coupling coefficient uncertainties compared to the respective uniform locking solutions. We also draw the reader's attention to the fact that although in this paper we present and discuss only the block model results for the upper plate structures, in all inversion runs we simultaneously estimated the angular velocities and the locking parameters of the Hellenic subduction system features (i.e., the plate interface and the Hellenic and Ptolemy trough faults) which comprise the topic of the companion article (Chousianitis et al., 2026). An interesting feature in Figure 9b is the presence of coherently NE-directed elastic deformation surface velocities across southern Peloponnese, observed not only near block-bounding faults but also at distances away from them. This pattern can be attributed to the presence of coupled patches along the western segment of the Hellenic subduction system (a feature i.e. analyzed in the companion article; Chousianitis et al., 2026) which influence the elastic strain accumulation in the overriding plate.

6. Inversion Results and Interpretation

6.1. Geodetic Fault Slip Rates

The preferred model matches the data reasonably well in terms of the sense of slip on the active faults that separate the blocks. The only block boundary on which the relative motion direction wasn't initially consistent with what expected from geology was the Atalanti fault (No. 10 in Table S4 and Figure S2 of Supporting Information S1), one of the very few active faults of Greece with an estimated long-term geological slip rate. To this end, we forced all models (i.e., our best fit model and those presented in Text S1 of Supporting Information S1) to satisfy 0.57–2.49 mm/yr fault-normal slip in accordance with the range of values proposed by Pantosti et al. (2004). The predicted geodetic fault slip rates from our best fit kinematic model are presented in Figure 8a and are tabulated in Table S4 of Supporting Information S1, while the corresponding fault-normal and fault-parallel slip rate components for each fault segment are illustrated in Figures 8b and 8c, respectively. If we exclude the Hellenic subduction system features which are the subject of the companion article (Chousianitis et al., 2026), the upper plate faults have geodetic slip rates which range between 0.5 and 19.4 mm/yr, while most of them exceed 4–5 mm/yr. Given the high slip rates which characterize the majority of these faults, it is expected that elastic transients play a significant role in interseismic deformation within the study area. This is confirmed by the test that we described in the last paragraph of the previous section, where, assuming no coupling across all block-bounding faults we obtained poor fits, indicating that the effect of elastic strain accumulation to the present-day deformation patterns is important and should be taken into account when kinematic models are used to reproduce geodetic data.

The highest slip rates were resolved at the large strike-slip structures which transect the north Aegean Sea and western Greece, namely the NAF (No. 1 in Table S4 and Figure S2 of Supporting Information S1), the CTFZ (No. 34 in Table S4 and Figure S2 of Supporting Information S1) and the Kato Achaia-Amaliada Fault Zone (KAFZ; No. 39 in Table S4 and Figure S2 of Supporting Information S1). Model slip rates on the section of the NAF which extends from longitude 25°E to 30°E, show an average of 19 ± 0.4 mm/yr of right-lateral strike-slip motion (all uncertainties reported in the text correspond to formal 1-sigma confidence intervals). Also based on GPS, Briole et al. (2021) estimated a rate of ∼15 mm/yr, while Le Pichon and Kreemer (2010), Özbey et al. (2021), Pérouse et al. (2012) and Reilinger et al. (2006) reported rates between 19 and 26 mm/yr. The lower slip rate inferred by Briole et al. (2021) most likely reflects the very sparse GPS velocity field available at the time of that study, particularly along the northern Aegean islands, combined with their adoption of a curved fault surface that differs from the planar segment representation used here. As we move westwards, the change in the strike of the fault segments that define the westernmost part of the NAT and the SE margin of the adjacent NAB is accompanied by a decrease in the strike-slip motion which becomes ∼13.5 ± 0.7 mm/yr. However, west of longitude 23.8°E, where the block boundary turns into a NW-SE direction, model slip rates suggest that the southwestern margin of the NAB accommodates predominantly extension at an average rate of 8 ± 0.7 mm/yr which is coupled with a low strike-slip rate of 2.5 ± 0.6 mm/yr. This different kinematic behavior of the western half of the NAB, which implies that it is controlled by extensional rather than strike-slip tectonics, was also revealed through geodetic strain rate mapping (Chousianitis et al., 2024).

Regarding the major strike-slip structures of western Greece, our best fit model predicts that slip rates on the CTFZ decrease southwestwards from 19.3 ± 0.6 mm/yr west of Lefkada island to 16 ± 0.9 mm/yr west of

21699356, 2026, 7, Downloaded from https://agupubs.onlinelibrary.wiley.com/doi/10.1029/2025JB033218, Wiley Online Library on [04/07/2026]. See the Terms and Conditions (https://onlinelibrary.wiley.com/terms-and-conditions) on Wiley Online Library for rules of use; OA articles are governed by the applicable Creative Commons License

Cephalonia island. In the latter case, the remaining slip rate budget of the CTFZ appears to be accommodated by the strike slip fault which extends onshore the western peninsula of Cephalonia island in a sub-parallel direction to the CTFZ. Accordingly, we estimate a 2.6 ± 0.8 mm/yr of right-lateral slip on this fault, which if we add to the 16 ± 0.9 mm/yr of the CTFZ west of Cephalonia island, will equate the slip rate of the CTFZ west of Lefkada island. In this context, it seems that slip in the Cephalonia part of the CTFZ is divided between the CTFZ and the onshore Paliki fault (No. 35 in Table S4 and Figure S of Supporting Information S12). Previous estimates of the slip rate of the CTFZ ranged from 15 mm/yr (Vassilakis et al., 2011) to 19.7 mm/yr (Vernant et al., 2014), although the calculations in these studies correspond to the entire length of the fault zone. As regards the KAFZ in NW Peloponnese which comprises the second most important strike-slip structure in western Greece, previous results concerning the slip rate are contradictory. Vernant et al. (2014) estimated 8.9 mm/yr right-lateral strike-slip motion and 8.6 mm/yr extension (i.e., oblique-slip behavior), while Briole et al. (2021) resolved a strike-slip rate of 7.4 mm/yr and a shortening rate of 2.3 mm/yr. On the contrary, our model predicts that the KAFZ accommodates 15.0 ± 0.9 mm/yr of right-lateral slip, with no additional component of boundary-normal motion, consistent with the pure strike-slip nature of the 8 June 2008 earthquake which revealed the existence of this fault zone that had remained, until then, unknown. Interestingly, our model resolved a significant right-lateral slip rate of 13.0 ± 0.6 mm/yr at the Oraeoi Strait (No. 9 in Table S4 and Figure S2 of Supporting Information S1), implying that this NE-SW trending morphological structure comprises a zone of strike-slip tectonics extending toward central Greece. This aligns with Porkoláb et al. (2023) who suggested that dextral shear localization is proceeding beyond the SW termination of the northern branch of the NAF and may eventually evolve into a dextral boundary zone. Furthermore, contrary to the previously prevailing view, active shear deformation has been observed to extend toward Evia and central Greece, as revealed by recent strike-slip earthquake swarms and sequences in the region (Sboras et al., 2025).

Lower slip rates were resolved along the remaining block-bounding faults for which our model predicted strike-slip motion. In this context, along the southern branch of the NAF we estimated a right-lateral slip rate that ranges from 3.8 to 5.4 ± 0.4 mm/yr with the exception of its SW tip, where the strike-slip rate increases to 7.5 ± 0.7 mm/yr. In this area, our model also predicts that the Skyros fault, which acts as the conjugate to the southern branch of the NAF, has a left-lateral slip rate of −7.6 ± 0.6 mm/yr coexisting with a small extensional component of 4.0 ± 0.5 mm/yr. We also estimate an average of 8.0 ± 0.6 mm/yr of right-lateral slip on the Sigacik-Seferihisar fault at western Turkey (No. 8 in Table S4 and Figure S2 of Supporting Information S1). The remaining strike-slip boundaries are located in NW Greece and Albania. Among them, the most important is the Katouna-Stamna fault zone, where our best fit model predicts a left-lateral slip rate of −9.4 ± 0.7 mm/yr, similar to that estimated by Pérouse et al. (2017) and Briole et al. (2021). Farther north, we find sinistral slip rates of −1.7 ± 2.4 mm/yr for the Petoussi fault (No. 41 in Table S4 and Figure S2 of Supporting Information S1) and dextral slip rates of 7.7 ± 3.8 mm/yr for the Qeparo Transfer Fault is southern Albania (No. 42 in Table S4 and Figure S2 of Supporting Information S1). Despite the high uncertainties on the slip rate estimates of these two faults, which are attributed to the few GPS data within the respective blocks, their sense of motion has been correctly estimated. For the dextral Lushnje Transfer Fault in central Albania (No. 43 in Table S4 and Figure S2 of Supporting Information S1) we find an average of 3.8 ± 0.8 mm/yr of strike-slip motion along with a minor extensional component of 1.5 ± 0.7 mm/yr.

The majority of the block-bounding faults of our model exhibit extensional and oblique-extensional kinematics. In central Greece, model slip rates across the Gulf of Corinth show 13.7 ± 0.8 mm/yr of almost pure extension, grossly compatible with the opening rates of the Corinth Rift which range from 10 mm/yr to 16 mm/yr at its eastern and western part, respectively (Avallone et al., 2004; Briole et al., 2000; Chousianitis et al., 2013). Toward the ENE, across the block boundaries that are defined by the normal faults of Perachora, and Kaparelli-Erithres (No. 19 and 20 in Table S4 and Figure S2 of Supporting Information S1), we estimate smaller but considerable amounts of extension on the order of 6.0 ± 0.8 mm/yr and 9.0 ± 0.9 mm/yr, respectively. On the contrary, to the ESE of the Corinth Rift, the model gives a very low extensional slip rate of 0.9 ± 0.6 mm/yr across the block boundary that is defined by the Loutraki fault (No. 22 in Table S4 and Figure S2 of Supporting Information S1). To the west of the Corinth Rift our model predicts an extensional slip rate of 9.2 ± 0.7 mm/yr across the Patras Gulf revealing that the crustal extension which controls the Corinth Rift continues beyond its western termination. The Patras Gulf extensional rate along with its direction are almost equal to the slip rate of the NNW-SSE trending Katouna-Stamna fault zone implying that the extension of the Patras Gulf is transferred to the Katouna-Stamna fault zone. Moreover, our model predicts a significant extensional rate across the Amvrakikos Gulf of

21699356, 2026, 7, Downloaded from https://agupubs.onlinelibrary.wiley.com/doi/10.1029/2025JB033218, Wiley Online Library on [04/07/2026]. See the Terms and Conditions (https://onlinelibrary.wiley.com/terms-and-conditions) on Wiley Online Library for rules of use; OA articles are governed by the applicable Creative Commons License

14.8 ± 0.8 mm/yr. This extension occurs because both tips of the E-W trending Amvrakikos Gulf comprise intersections with large strike-slip structures, namely the dextral CTFZ and the sinistral Katouna-Stamna fault zone, which transfer their motion at the western and eastern part of the Amvrakikos Gulf and induce its opening.

In northern Greece, our model predicts a pure extensional slip rate of 7.2 ± 0.4 mm/yr along the boundary that is defined by the Belles and Lakavica normal faults (No. 15 in Table S4 and Figure S2 of Supporting Information S1). Along the nearby Strymon fault system (No. 16 in Table S4 and Figure S2 of Supporting Information S1), model slip rates show N-directed oblique (left-lateral) extension at 6.5 ± 0.4 mm/yr. Other notable boundaries where our best fit model predicted extensional or oblique-extensional slip rates were found throughout eastern Aegean. In this context, we estimate pure extension with a slip rate of 3.8 ± 0.5 mm/yr across the Chios fault (No. 7 in Table S4 and Figure S2 of Supporting Information S1) and oblique extension with an average slip rate of 8.5 ± 0.5 mm/yr across the Ikaria and Samos Basin faults (No. 25 and 26 in Table S4 and Figure S2 of Supporting Information S1). Farther south, our model predicts a pure extensional slip rate of 8.6 ± 0.6 mm/yr for the Kos fault (No. 27 in Table S4 and Figure S2 of Supporting Information S1) and an oblique extensional slip rate of 13.5 ± 0.7 mm/yr across the Gökova fault zone (No. 30 in Table S4 and Figure S2 of Supporting Information S1), where previous geodetic estimates vary significantly from 4.9 mm/yr (Vernant et al.,. 2014) to 20.2 mm/yr (Reilinger et al., 2006). To the south of Kos island, the NNW-SSE trending boundary that passes west of Karpathos and Kasos islands and terminates offshore eastern Crete (No. 28 in Table S4 and Figure S2 of Supporting Information S1) accommodates a slightly oblique extension at a rate of 9.3 ± 0.6 mm/yr (2.9 mm/yr of strike-slip motion and 8.8 mm/yr of fault normal motion) trending ~N49°W, in good agreement with the average slip rate of 8.6 mm/yr (3.7 mm/yr of strike-slip motion and 7.8 mm/yr of fault normal motion) estimated by Vernant et al. (2014). To the east of Rhodes, the NE-SW trending boundary of our block model which follows the steep seafloor escarpment between the island and the Rhodes Basin (Woodside et al., 2000; No. 29 in Table S4 and Figure S2 of Supporting Information S1), shows a transpressional motion of 18.6 ± 1.2 mm/yr among which 17.6 mm/yr correspond to sinistral strike-slip motion and 6.1 mm/yr to shortening. This sense of motion was also resolved by Reilinger et al. (2006) and Vernant et al. (2014), although with quite different average rates, that is 35 mm/yr (33.9 mm/yr of sinistral motion and 8.7 mm/yr of shortening) and 13.7 mm/yr (13.1 mm/yr of sinistral motion and 4.1 mm/yr of shortening), respectively.

Finally, if we exclude the boundaries associated with the Hellenic subduction system (i.e., the plate interface and the Hellenic and Ptolemy trough faults) which are discussed in the companion article (Chousianitis et al., 2026), our model predicts compressional motions only across the boundaries that define the Aegean-Apulian Collision Zone (AACZ). At the part of the AACZ that is located offshore NW Greece, Corfu and southern Albania, we estimated a slip rate of 7.6 ± 0.6 mm/yr with a slip direction of N114°W. This direction is almost the same with the one reported in Louvari et al. (2001) using seismological evidence. As regards the predicted rate of our best fit model, it is higher than the rate of 5 mm/yr reported in Pérouse et al. (2012) but smaller than the rate of 8.9 mm/yr estimated by Valkaniotis et al. (2020). Further north however, offshore central Albania, our model predicts that the collision between the Apulian platform with Eurasia changes in rate and direction. In this context, slip rate decreases to 4.1 ± 1.1 mm/yr and slip direction becomes highly oblique with an azimuth of N150°W.

6.2. Fault Locking Estimates and Slip Rate Deficits

In our best fit model, the estimated coupling coefficients φ had low formal errors which in almost all cases were below 0.5. Only a few small block boundary faults had φ values with errors greater than 0.5 and in those cases, we fixed them at either 0.0 or 1.0 depending on whether the φ estimate was closer to 0.0 or 1.0. Such large uncertainties occurred for the Loutraki and Chios faults, which we fixed at $\varphi = 1.0$ and $\varphi = 0.0$, respectively. The coupling coefficients on the majority of the block-bounding faults of our best fit model fall between 0.5 and 1.0, indicating partially locked or fully locked structures (Figure 10a). These φ values multiplied by the long-term slip rate along the faults give the slip rate deficits, which is a measure of their accumulating elastic strain (Figure 10b). We note here that to assess the sensitivity of the locking estimates to fault dips, we performed two tests in which the dip angles of all normal and reverse faults were increased by +10° in one case and decreased by −10° in the other. The results of these tests indicated that differences in fault locking estimates are within the uncertainties, confirming that such variations in fault dips have a limited impact on the obtained coupling coefficients.

Model results show low coupling ($\varphi \sim 0.3$) across the section of the northern branch of the NAF that extends from longitude 25°E to 30°E, a zone that has been the source of several large (>6.0) earthquakes. We note, however,

21699356, 2026, 7, Downloaded from https://agupubs.onlinelibrary.wiley.com/doi/10.1029/2025JB033218, Wiley Online Library on [04/07/2026]. See the Terms and Conditions (https://onlinelibrary.wiley.com/terms-and-conditions) on Wiley Online Library for rules of use; OA articles are governed by the applicable Creative Commons License

10.1029/2025JB033218

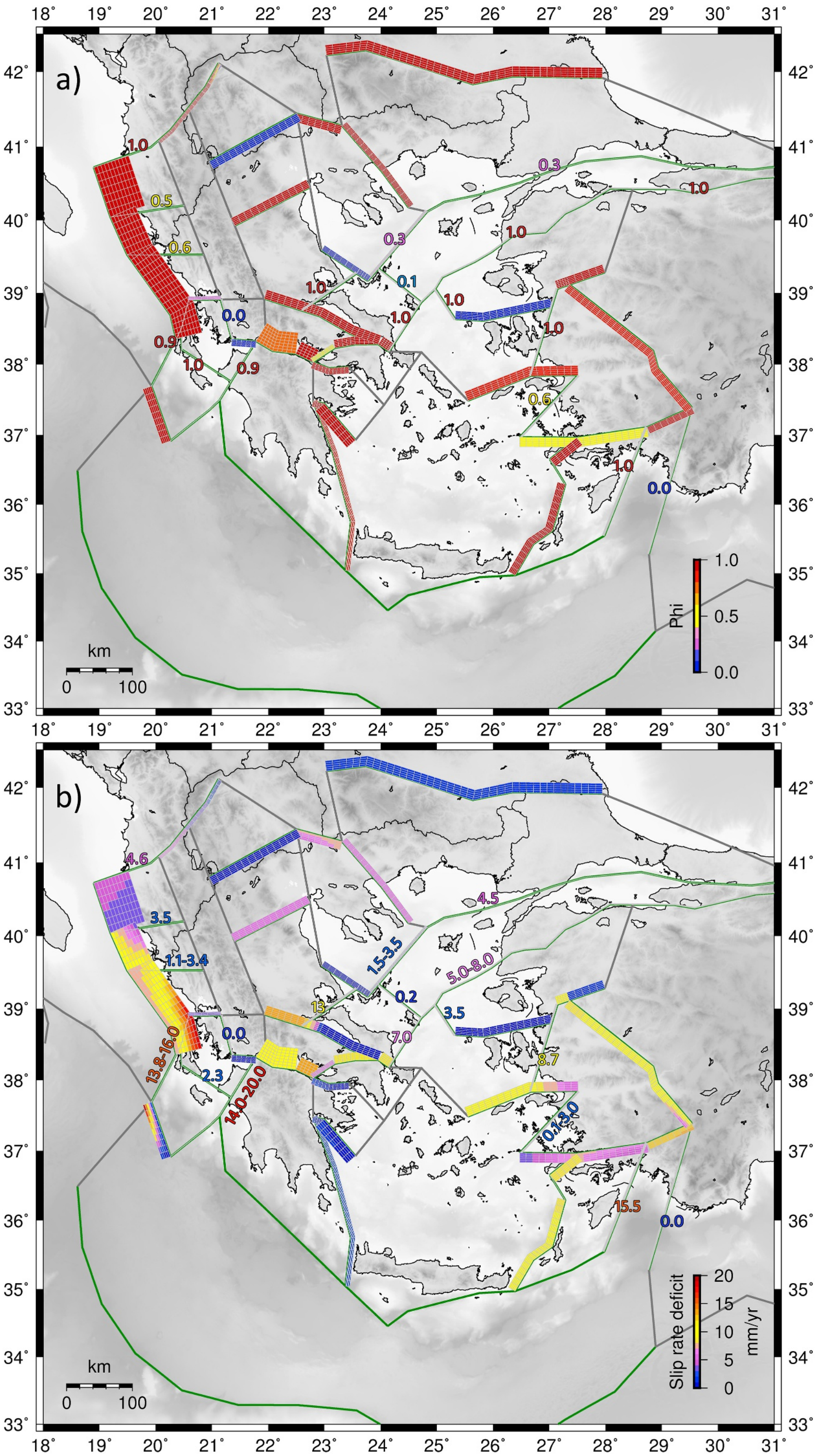

Figure 10. (a) Coupling coefficients φ and (b) slip rate deficits on block-bounding faults of the best fit model. For vertical faults whose plane is not visible in map view, the coupling coefficients and the slip rate deficits are shown as numbers colored according to the respective color bars.

21699356, 2026, 7, Downloaded from https://agupubs.onlinelibrary.wiley.com/doi/10.1029/2025JB033218, Wiley Online Library on [04/07/2026]. See the Terms and Conditions (https://onlinelibrary.wiley.com/terms-and-conditions) on Wiley Online Library for rules of use; OA articles are governed by the applicable Creative Commons License

that this value corresponds to the average calculated coupling coefficient for the entire fault area and acknowledge that significant variations across its length should be expected due to the presence of fully locked asperities together with partially locked and unlocked sections, especially across the Marmara Sea section (Karabulut et al., 2011). Our model predicts that from longitude 25°E to 30°E the NAF has an average slip rate deficit of 4.5 mm/yr. The slip rate deficit can be used to estimate the corresponding moment accumulation rate using the formula $\dot{M}_0 = \mu \sum S_d A$, where μ is the shear modulus (taken as 30 GPa), S_d is the slip rate deficit and A is the fault sub-segment area. In this way, and excluding the Marmara Sea section, we found a moment accumulation rate of 3.6×10^{17} N m/yr for the offshore section that is extending along the NAT, which is equivalent to the moment released by a M_w 7.0 earthquake every 97 years. Model coupling across the section of the northern branch to the west of longitude 25°E, remains low ($\varphi \sim 0.3$). At this section, which outlines the westernmost part of the NAT and the SE margin of the NAB, the slip rate deficit decreases compared to what we found east of 25°E, exhibiting a westward drop from 3.5 mm/yr to 1.5 mm/yr. These deficits correspond to a moment accumulation rate of 2.6×10^{17} N m/yr, so at this section of the northern branch of the NAF, a larger recurrence time of 139 years is required to produce a M_w 7.0 earthquake.

We estimate full locking on the southern branch of the NAF and slip rate deficits which vary from 5 mm/yr to 8 mm/yr (average of 5.5 mm/yr). The western termination of this branch was the source of a M_w 6.9 earthquake in 1981 (Makropoulos et al., 2012). At these slip rate deficits, the entire offshore section of the southern branch of the NAF accumulates moment at a rate of 1.18×10^{18} N m/yr, while its western termination that ruptured during the 1981 event accumulates 1.87×10^{17} N m/yr, which is equivalent to a recurrence rate of one M_w 6.9 event every ~130 years. Most of the block-bounding faults along the eastern Aegean Sea and the western coastline of Turkey show either full coupling (i.e. the Sigacik-Seferihisar fault, the Karpathos and Kasos offshore faults, the Kos fault, and the Rhodes Basin fault) or display a high level of coupling (i.e. the Ikaria and the adjacent Samos Basin fault, with a φ value of 0.8). We observe significant fault slip rate deficits along all of these faults. Notably, the Kos fault has an average slip rate deficit of 8.5 mm/yr, the Kasos fault has 9.3 mm/yr and the Sigacik-Seferihisar fault has 8.7 mm/yr. The deficit in slip rate of the Ikaria fault increases westward from 8 mm/yr to 10 mm/yr, while that of the Samos Basin fault increases westward from 5 mm/yr to 7 mm/yr. Finally, the Rhodes Basin fault exhibits an average slip rate deficit of 15.5 mm/yr. The segment of this fault which, according to Howell et al. (2015), ruptured by an earthquake of $M_w \geq 7.7$ and caused the Holocene uplift of Rhodes, accumulates moment at a rate of 2.8×10^{17} N m/yr. At this rate, earthquakes of M_w 7.8–7.9 would have recurrence intervals of ~2000–2800 years, implying single-event slips of ~30–40 m. Although these slip values are large, they are consistent with the estimates of Howell et al. (2015) who indeed considered slip of that magnitude and placed the occurrence of such events between 2000 BC and 200 BC.

Significant slip rate deficits were also resolved along many of the block-bounding faults in central Greece. For the boundaries that outline the western and eastern part of the Corinth Rift we obtained φ values of 0.7 and 1.0 and average slip rate deficits of 10 mm/yr and 13.5 mm/yr, respectively. These values highlight that at present the eastern part accumulates strain, and therefore seismic moment, at a higher rate compared to the western part. This can be attributed to the much more intense seismic activity that affects the western part of the rift, resulting in quicker seismic moment release and consequently in smaller accumulation of elastic strain. Indeed, the increased microseismicity, the occurrence of the M_w 6.4 Aigio earthquake in 1995 and the frequent swarms (in 2001, 2003, 2010, 2013, 2020) of the western part have contributed to the seismic release of some fraction of the accumulated elastic strain, contrary to the much quieter eastern part. Further east, the block boundary which is associated with the ruptures of the three $M_s > 6.4$ earthquakes in 1981 within the Alkyonides Gulf (No. 19 in Table S4 and Figure S2 of Supporting Information S1) has an average slip rate deficit of 5 mm/yr and is characterized by partial coupling ($\varphi = 0.5$). The eastward continuation of this block boundary, however, which is defined by the ENE-WSW trending normal faults in Viotia (notably the Kaparelli-Erithres fault zone) and the SE-NW trending normal faults that delineate the southern margin of the South Evia Gulf (notably the Oropos fault), appears fully locked with a significant average slip rate deficit of 11 mm/yr.

Regarding the major block boundary in central Greece which is defined by the Atalanti and the Sperchios valley faults, our data require full locking. The slip rate deficit, however, along the former is considerably smaller because of the hard constraint for a slow slip rate which we imposed (see Section 6.1). The Atalanti fault is well-known for the occurrence of two successive $M > 6$ earthquakes in 1894, although their magnitude estimates vary significantly and range from M 6.4 to 6.7 for the first event and from M 6.5 to 7.0 for the second event (Albini &

21699356, 2026, 7, Downloaded from https://agupubs.onlinelibrary.wiley.com/doi/10.1029/2025JB033218, Wiley Online Library on [04/07/2026]. See the Terms and Conditions (https://onlinelibrary.wiley.com/terms-and-conditions) on Wiley Online Library for rules of use; OA articles are governed by the applicable Creative Commons License

Pantosti, 2004; Papazachos & Papazachou, 2003). Assuming that the entire moment deficit accumulation rate which is derived by our model is released by the 1894 earthquakes, we get a recurrence interval of ∼240 years for the events estimated by Albini and Pantosti (2004) and ∼1050 years for the events estimated by Papazachos and Papazachou (2003).

We estimate full coupling along the major strike-slip faults of western Greece, namely the CTFZ and the KAFZ, but very low to no coupling along the smaller strike-slip structures, namely the Paliki fault and the Katouna-Stamna fault zone, where coupling coefficients were found equal to 0.2 and 0.0, respectively. Particularly for the Katouna fault, our estimate that the fault is completely uncoupled implies that it primarily releases its tectonic energy through creep. This conclusion agrees with geological evidence for the creeping behavior of this fault presented in Pérouse et al. (2017), as well as with the large discrepancy between geodetic strain and earthquake moment release in the broader area presented in Chousianitis et al. (2015). No coupling was also estimated along the Stamna fault, which is the southward continuation of the Katouna fault, and along the boundary which delineates the north margin of the Patras Gulf, implying that the opening of the Patras Gulf takes place largely via creep, while very low coupling ($\varphi = 0.2$) was resolved along the Amvrakikos Gulf.

As regards the CTFZ and specifically its Lefkada segment, the M_w 6.5 earthquake in 2015 broke the part of the fault that remained unbroken during the M_w 6.2 earthquake in 2003, confirming that these two events ruptured the entire segment (Chousianitis et al., 2016). Our block model predicts a moment accumulation rate of 1.9×10^{17} N m/yr across this ∼50 km section of the CTFZ. At this rate, the recurrence interval of earthquakes capable to break the entire Lefkada segment (like those in 2003 and 2015) is estimated to be ∼45 years. Considering that prior to the 2003 and 2015 events, the Lefkada segment ruptured in 1948 by two M_w 6.5 earthquakes (Makropoulos et al., 2012), whose recurrence interval for the same moment accumulation rate is ∼65 years, it is plausible to assume that the Lefkada segment releases its accumulated elastic strain every 55 ± 10 years. The Cephalonia segment of the CTFZ has also been the source of large magnitude earthquakes during the instrumental period. If we exclude the four $M_w > 6.0$ events of 1953, whose association with the CTFZ is a matter of debate, the Cephalonia segment was ruptured by a M_w 6.0 earthquake in 1972 and by a M_w 6.7 earthquake in 1983 which was followed by a M_w 6.0 aftershock. The block model yields a moment accumulation rate of 2.2×10^{17} N m/yr, so assuming that the entire slip deficit is to be released by a seismic sequence like the one in 1983, we get a recurrence time of ∼62 years.

In NW Greece, model results show a coupling coefficient of 0.6 along the Petoussi fault and very strong ($\varphi = 0.9$) to full coupling ($\varphi = 1.0$) along the AACZ where the Apulian platform collides with the Aegean plate with shortening rates on the order of 7.6 mm/yr (see Section 6.1). This collision, which has been taking place offshore Albania-NW Greece since the early Pliocene (∼4–5 Ma), is associated with a subducting continental slab of ∼20 km thickness and of early Miocene age (∼20–25 Ma) that has been detected through scattered wave imaging (Pearce et al., 2012). Instrumental seismicity related to the ongoing upper plate thrusting in the vicinity of the AACZ is of small to moderate magnitude with low activity rates and very few instrumentally recorded $M_w > 5.0$ events (the most recent one being a $M_w = 5.4$ in 2007), while even lower activity is observed at intermediate depths supporting the presence of an almost seismically inactive subducting slab (Bocchini et al., 2018; Halpaap et al., 2018). Given the low level of seismicity associated with the AACZ, the very strong to full coupling that is predicted by the block model is surprising, because the implied large amounts of accumulated elastic strain susceptible of being released seismically somewhat contradict the relative quiescence over the last 100 years. However, despite the absence of major earthquakes during the instrumental era, historical seismicity evidences the occurrence of two $M = 7.0$ events in 1444 and 1743 as well as a $M = 6.6$ event in 1786 (Papazachos & Papazachou, 2003). In this context, the combination of a very high level of coupling with low seismic activity across the AACZ may be justified either by high frictional strength which inhibits the upcoming ruptures, or by very long recurrence times, which are reasonable enough since if we use the predicted moment deficit accumulation rate of 1.5×10^{17} N·m/yr we get recurrence intervals of ∼240 and ∼340 years for M_w 7.0 and 7.1 earthquakes, respectively. Of course, a combination of the aforementioned possibilities is also plausible, if not more likely.

6.3. Block Motions in the Aegean

When tectonic deformation is analyzed by means of elastic block models, the motions of crustal blocks are inferred from their angular velocities and correspond to the movement induced by their rigid rotations. Many of

21699356, 2026, 7, Downloaded from https://agupubs.onlinelibrary.wiley.com/doi/10.1029/2025JB033218, Wiley Online Library on [04/07/2026]. See the Terms and Conditions (https://onlinelibrary.wiley.com/terms-and-conditions) on Wiley Online Library for rules of use; OA articles are governed by the applicable Creative Commons License

Table 1
Angular Velocities for the Blocks of the Best-Fitting Model

Block	Longitude (°)	Latitude (°)	Omega (°/Myr)	Sig omega (°/Myr)	E_{max}	E_{min}	Azi
SDod	51.125	25.964	0.7744	0.2269	10.02	0.31	122.36
MedR	47.584	16.508	0.3245	0.0797	11.83	0.63	137.52
Argo	75.685	−9.599	0.3213	0.2023	81.12	0.66	137.34
CAeg	55.947	12.387	0.4862	0.0481	6.07	0.23	135.17
Atti	74.816	−7.072	0.3216	0.2728	87.03	0.49	137.64
Pelo	65.364	−2.035	0.3837	0.0850	25.02	0.36	139.46
CIon	40.184	26.516	0.5519	0.4316	22.33	0.37	131.22
CoGu	63.611	1.368	0.2473	0.1923	64.96	0.72	139.88
Aito	−106.479	44.751	−0.1318	0.0493	6.96	1.81	38.12
AnGr	51.117	9.642	0.4564	0.1302	16.12	0.34	146.92
Evia	86.884	−25.471	0.1918	0.0127	72.12	1.04	135.73
Chio	51.478	−1.684	0.3096	0.1904	46.57	0.71	152.30
NIon	−41.911	70.909	−0.0984	0.3206	2.80	2.86	101.08
Corf	23.793	30.807	0.5190	2.2814	50.42	1.04	161.57
Lesv	51.326	−17.671	0.2417	0.0529	30.84	0.57	159.10
Thes	54.347	27.392	0.1700	0.1725	41.84	0.84	123.25
NAeg	34.993	20.673	0.4771	0.0637	4.11	0.27	162.59
Vlor	21.318	39.359	1.0587	0.8902	1.86	0.18	143.86
ThTu	29.111	36.589	0.0995	0.0317	2.46	1.08	164.66
WMak	−68.619	6.807	−0.0386	0.0153	12.21	3.66	49.60
CMak	78.927	23.205	0.0872	0.1516	90.27	1.70	124.44
Pind	24.642	37.433	0.6622	0.3218	2.77	0.43	131.96
RNMa	24.868	41.347	0.5709	0.3258	2.30	0.38	88.07
IBas	55.719	7.872	0.2512	0.0696	20.31	0.80	138.95
Nubi	−19.494	1.777	0.0737	0.0029	2.84	1.41	27.84
Anat	32.111	31.283	1.2991	0.0181	0.15	0.08	171.72

Note. Longitude, latitude, and omega give the rotation poles and their associated rotation rates relative to Eurasia. Sig Omega is the standard error of the rotation rate. E_{max}, E_{min} and Azi are the error ellipse parameters.

these rotations in our case occur about distant poles which are located far from the study area (Table 1). The location of a pole with respect to its block depends on the rotational component of the velocity field (i.e., velocities with the short-term elastic part removed) that is estimated across the block. Blocks exhibiting uniform motion throughout their extent with velocities of the same direction and magnitude have distant poles, while blocks displaying a rotational pattern in the directions of their velocities and/or variability in their magnitudes, have nearby poles. Hence, the estimated distant poles imply that many of the Aegean blocks of the best fit model move coherently and have small internal rotations. Pole locations and their associated rotation rates (omega) are highly correlated parameters, so that given a specific block movement, a change in pole location will result in a relative change in the rotation rate in order for the predicted block motion to remain the same. In this context, block motions (i.e., movement induced by their rotations) of an elastic block model convey more meaningful information about tectonics and can be straightforwardly compared with estimates of other block models, than angular velocity parameters. The predicted motions at the centroids of each crustal block of our best fit model are depicted in Figure 11.

The highest predicted rates of motion occur on blocks which lie south of an axis that follows the NAF, traverses central Greece and reaches the central Ionian islands (Figure 11). Block velocities at this part of the Aegean range from 19 mm/yr to 35 mm/yr. The predicted motion of the two blocks bounded by the NAF and its northern and

21699356, 2026, 7, Downloaded from https://agupubs.onlinelibrary.wiley.com/doi/10.1029/2025JB033218, Wiley Online Library on [04/07/2026]. See the Terms and Conditions (https://onlinelibrary.wiley.com/terms-and-conditions) on Wiley Online Library for rules of use; OA articles are governed by the applicable Creative Commons License

10.1029/2025JB033218

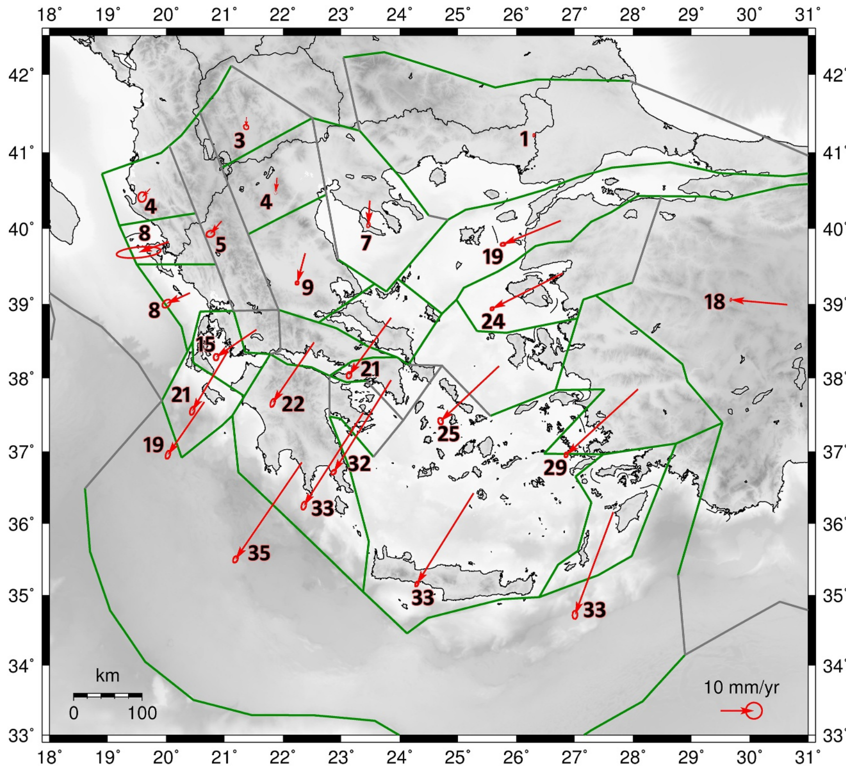

Figure 11. Predicted motion relative to Eurasia at the centroid of each crustal block of our best fit model inferred from their angular velocities. Numbers next to the arrows represent velocity magnitudes in mm/yr. Uncertainty ellipses correspond to the 95% confidence level.

southern branches within the Aegean is roughly parallel to the trend of these structures, with velocities of 19 and 24 mm/yr. The remaining fast-moving blocks of central-southern Aegean Sea and Peloponnese display a SW direction of motion with magnitudes which increase trenchwards, reaching 35 mm/yr. The Rhodes block deviates slightly from this SW direction, exhibiting a SSW motion, and given the velocities of its adjacent block to the north (29 mm/yr to the SW) and the Anatolia block (18 mm/yr to the WNW), it is evident that these blocks jointly undergo a counterclockwise rotation. Predicted velocities of the blocks which lie north of the aforementioned axis are much lower compared to those located to the south, ranging from 1 mm/yr to 9 mm/yr. Northeastern Greece appears to be part of stable Eurasia since its inferred block motion is merely 1 mm/yr. Toward the west, the SSW-oriented motion of central and western Macedonia transitions to a gradual rotation of the velocities of the central and NW Greece blocks to the west.

Overall, Figures 9a and 11 indicate that crustal blocks in the Aegean can be classified into two categories, separated by a boundary that follows the NAF, crosses central Greece, and terminates in the central Ionian islands. Fast-moving blocks with distant poles are located south of this boundary, while slower-moving blocks with nearby poles lie to the north. The second notable kinematic feature of the block model is the opposing rotations of central-NW Greece (clockwise) and SE Aegean-SW Anatolia (counterclockwise). These kinematic patterns result from large-scale plate tectonic processes that in some cases operate in conjunction within the Aegean, including transition from subduction to collision, tectonic escape, slab rollback and trench retreat. Critical roles in block kinematics are from the westward tectonic escape of Anatolia and the fast slab rollback at the Hellenic subduction zone. Regardless of whether, or to what extent, slab rollback contributes to the lateral extrusion of Anatolia, both of these mechanisms are responsible for the southwestward motion and the trenchward-increasing velocities of the fast-moving blocks of the Aegean Sea and Peloponnese. The counterclockwise rotation of the SE Aegean-SW Anatolia blocks is likely driven by the substantial reduction in the convergence rate along the Hellenic-Cyprus subduction system east of Rhodes, where it decreases from ~35 mm/yr in SE Aegean to ~5 mm/yr near Cyprus. Due to this rate difference, the pulling forces exerted on the upper plate by the rapid southward trench retreat along the Hellenic Arc are transmitted as far as the slab tear beneath SW Anatolia, which separates the

21699356, 2026, 7, Downloaded from https://agupubs.onlinelibrary.wiley.com/doi/10.1029/2025JB033218, Wiley Online Library on [04/07/2026]. See the Terms and Conditions (https://onlinelibrary.wiley.com/terms-and-conditions) on Wiley Online Library for rules of use; OA articles are governed by the applicable Creative Commons License

Hellenic and Cyprus Arcs. To the east of this boundary, the upper plate is no longer required to accommodate the rapid trench retreat, so the pulling forces driving the upper plate toward the subduction zone cease, resulting in the counterclockwise rotation of the SE Aegean-SW Anatolia blocks. Finally, clockwise rotation of the tectonic blocks of central-NW Greece is associated with the rapid southwestward movement of the Aegean Sea and Peloponnese blocks, as well as the changing conditions of the Nubia-Eurasia plate boundary in western Greece, where, north of the central Ionian islands, the tectonic regime shifts from oceanic subduction to continental collision/subduction. This change causes a pronounced rate difference between the slow collision of the thick and buoyant continental lithosphere across NW Greece and the fast convergence of the thin and less buoyant oceanic lithosphere further south, which is influenced by slab rollback as well. In this way, the strong collisional resistance forces along the Aegean-Apulian Collision Zone, combined with the rapid SW movement of the tectonic blocks of central Ionian Sea-SW Aegean and north Aegean Sea, generates a rotational torque on NW Greece, facilitating its clockwise rotation. This framework has been widely used to explain tectonic block rotations at several active plate boundaries, such as in New Zealand (Wallace et al., 2004), the Pacific Northwest (McCaffrey et al., 2007) and elsewhere (Wallace et al., 2005), and it appears to represent a significant mechanism driving the rotation of central-NW Greece as well.

7. Conclusions

Using 832 GPS velocities and 146 earthquake slip vectors, we produced a region-wide kinematic block model which allowed us to evaluate the active tectonic setting of the Aegean region accounting for the effects of block rotation and elastic strain accumulation. The constructed model is compatible with the geometry of major known active faults and facilitated the estimation of fault slip rates and coupling ratios. For some of these faults we present geodetic slip rates and moment accumulation rates for the first time, while for others we provide updated and improved estimates. In addition to the GPS velocities, we used earthquake slip vector azimuths which brought useful constraints to some blocks with fewer GPS data.

In western Greece, our data suggest a fully coupled CTFZ with a dextral slip rate of 19.5 mm/yr. The Lefkada segment of the CTFZ accommodates the totality of this strike-slip motion, while to the south this motion is partitioned on the Cephalonia segment of the CTFZ (16 mm/yr) and the sub-parallel Paliki fault (2.6 mm/yr). To the north of the CTFZ, a contraction rate of 7.6 mm/yr at a pure frontal direction along the AACZ is responsible for the collision of the Apulian platform with Eurasia offshore NW Greece and southern Albania, while offshore central Albania, this rate decreases to 4.1 mm/yr and acquires a significant oblique component toward the SW. Slip rates along the NAF and its northern branch that is entering the north Aegean Sea vary laterally. We estimate average slip rates of 19 mm/yr of dextral strike-slip motion on the section that is extending from NW Turkey up to the western part of the NAT at longitude 25°E. Further west, across the westernmost part of the NAT and the SE margin of the NAB the amount of dextral slip rate predicted by our model decreases to ∼13.5 mm/yr, while west of longitude 23.8°E, the SW margin of the NAB exhibits both dextral and extensional deformation, but with rates which indicate the dominance of extensional motions (8 mm/yr) over the strike-slip component (2.5 mm/yr). Along the southern branch of the NAF we estimate lower right-lateral slip rates compared to those of the northern branch, ranging between 3.8 and 7.5 mm/yr.

Our data confirm the presence of strike-slip deformation beyond the SW termination of the northern branch of the NAF, toward central Greece, given that we found a dextral slip rate of 13 mm/yr along the Oraeoi Strait. At Peloponnese, the KAFZ accommodates significant right-lateral slip at a rate of 15 mm/yr and appears to be fully coupled, consistent with its significant seismic activity in recent times. The remaining block-bounding faults accommodate less than 10 mm/yr, but they are required to explain much of the data, especially in central Greece. We observed that crustal extension continues beyond the western termination of the Corinth Rift, into the Patras Gulf. Model results show that the Katouna-Stamna fault zone is completely uncoupled, while we found evidence for high slip rate deficits across the Corinth Rift, ranging between 10 mm/yr and 13.5 mm/yr. However, we note that these high deficit rates, which imply unreleased moment, are partially released by aseismic processes.

Model results suggest that crustal blocks in the SE Aegean-SW Anatolia undergo counterclockwise rotation, while those in central-NW Greece rotate clockwise. Between these opposing rotational domains, crustal blocks exhibit rapid southwestward motion with trenchward-increasing velocities. The observed block kinematics in the Aegean are primarily influenced by large-scale plate tectonic processes that in some cases act jointly to produce the present-day geodynamic framework. These include the westward tectonic escape of Anatolia, the fast slab

21699356, 2026, 7, Downloaded from https://agupubs.onlinelibrary.wiley.com/doi/10.1029/2025JB033218, Wiley Online Library on [04/07/2026]. See the Terms and Conditions (https://onlinelibrary.wiley.com/terms-and-conditions) on Wiley Online Library for rules of use; OA articles are governed by the applicable Creative Commons License

rollback and the rapid southward trench retreat along the Hellenic Arc, as well as the changing conditions along the Nubia-Eurasia plate boundary with the transition from oceanic subduction to continental collision/subduction north of the central Ionian islands and the substantial reduction in the convergence rate along the Hellenic-Cyprus subduction system east of Rhodes.

Conflict of Interest

The authors declare no conflicts of interest relevant to this study.

Availability Statement

The TDEFNODE control and input files that were used in this research and the final GPS velocity field are available at Chousianitis (2026). The computer code TDEFNODE that was used to model elastic lithospheric block rotations and locking on block-bounding faults is publicly available at McCaffrey (2023). Figures were made using GMT (Wessel et al., 2019), available at https://www.generic-mapping-tools.org.

Acknowledgments

We would like to thank the Editor, Anke Friedrich, for facilitating the simultaneous review process of this manuscript and its companion paper, and the Associate Editor for thoughtful guidance. We also express our appreciation to Andy Howell and an anonymous reviewer for their exceptionally thorough, insightful and constructive reviews, which greatly improved the quality and clarity of this paper. The publication of this article in OA mode was financially supported by HEAL-Link.

References

Albini, P., & Pantosti, D. (2004). The 20 and 27 April 1894 (locris, central Greece) earthquake sources through coeval records on macroseismic effects. *Bulletin of the Seismological Society of America*, *94*(4), 1305–1326. https://doi.org/10.1785/012003174

Allen, C. R. (1969). Active faulting in northern Turkey. In *Division of Geological Sciences California* (Vol. 1577). Institute of Technology. 32

Angelier, J., Lyberis, N., Le Pichon, X., Barrier, E., & Huchon, P. (1982). The tectonic development of the Hellenic arc and the Sea of Crete: A synthesis. *Tectonophysics*, *86*(1–3), 159–196. https://doi.org/10.1016/0040-1951(82)90066-X

Armijo, R., Lyon-Caen, H., & Papanastassiou, D. (1992). East-west extension and Holocene normal-fault scarps in the Hellenic arc. *Geology*, *20*(6), 491–494. https://doi.org/10.1130/0091-7613(1992)020<0491:eweahn>2.3.co;2

Armijo, R., Meyer, B., Hubert, A., & Barka, A. (1999). Westward propagation of the North Anatolian fault into the northern Aegean: Timing and kinematics. *Geology*, *27*(3), 267–270. https://doi.org/10.1130/0091-7613(1999)027<0267:WPOTNA>2.3.CO;2

Armijo, R., Meyer, B., King, G. C. P., Rigo, A., & Papanastassiou, D. (1996). Quaternary evolution of the Corinth Rift and its implication for the late Cenozoic evolution of the Aegean. *Geophysical Journal International*, *126*(1), 11–53. https://doi.org/10.1111/j.1365-246X.1996.tb05264.x

Avallone, A., Briole, P., Agatza-Balodimou, A. M., Billiris, H., Charade, O., Mitsakaki, C., et al. (2004). Analysis of eleven years of deformation measured by GPS in the Corinth Rift Laboratory area. *Comptes Rendus Geoscience*, *336*(4–5), 301–311. https://doi.org/10.1016/j.crte.2003.12.007

Barbot, S., & Weiss, J. R. (2021). Connecting subduction, extension and shear localization across the Aegean Sea and Anatolia. *Geophysical Journal International*, *226*(1), 422–445. https://doi.org/10.1093/gji/ggab078

Barka, A. A. (1992). The North Anatolian fault zone. *Annales Tectonicae*, *6*, 164–195.

Bell, R. E., McNeill, L., Bull, J. M., & Henstock, T. J. (2008). Evolution of the offshore western Gulf of Corinth. *Geological Society of America Bulletin*, *120*(1–2), 156–178. https://doi.org/10.1130/B26212.1

Benetatos, C., Kiratzi, A., Papazachos, C., & Karakaisis, G. (2004). Focal mechanisms of shallow and intermediate depth earthquakes along the Hellenic Arc. *Journal of Geodynamics*, *37*(2), 253–296. https://doi.org/10.1016/j.jog.2004.02.002

Bird, P. (2003). An updated digital model of plate boundaries. *Geochemistry, Geophysics, Geosystems*, *4*(3), 1027. https://doi.org/10.1029/2001GC000252

Bocchini, G. M., Brüstle, A., Becker, D., Meier, T., van Keken, P. E., Ruscić, M., et al. (2018). Tearing, segmentation, and backstepping of subduction in the Aegean: New insights from seismicity. *Tectonophysics*, *734*(735), 96–118. https://doi.org/10.1016/j.tecto.2018.04.002

Briole, P., Elias, P., Parcharidis, I., Bignami, C., Benekos, G., Samsonov, S., et al. (2015). The seismic sequence of January–February 2014 at Cephalonia Island (Greece): Constraints from SAR interferometry and GPS. *Geophysical Journal International*, *203*(3), 1528–1540. https://doi.org/10.1093/gji/ggv353

Briole, P., Ganas, A., Elias, P., & Dimitrov, D. (2021). The GPS velocity field of the Aegean. New observations, contribution of the earthquakes, crustal blocks model. *Geophysical Journal International*, *226*(1), 468–492. https://doi.org/10.1093/gji/ggab089

Briole, P., Rigo, A., Lyon-Caen, H., Ruegg, J. C., Papazissi, K., Mitsakaki, C., et al. (2000). Active deformation of the Corinth rift, Greece: Results from repeated Global Positioning System surveys between 1990 and 1995. *Journal of Geophysical Research*, *105*(B11), 25605–25625. https://doi.org/10.1029/2000JB900148

Brooks, M., Clews, J. E., Melis, N. S., & Underhill, J. R. (1988). Structural development of Neogene basins in western Greece. *Basin Research*, *1*(3), 129–138. https://doi.org/10.1111/j.1365-2117.1988.tb00010.x

Brüstle, A., Friederich, W., Meier, T., & Gross, C. (2014). Focal mechanism and depth of the 1956 Amorgos twin earthquakes from waveform matching of analogue seismograms. *Solid Earth*, *5*(2), 1027–1044. https://doi.org/10.5194/se-5-1027-2014

Caputo, R., Catalano, S., Monaco, C., Romagnoli, G., Tortorici, G., & Tortorici, L. (2010). Active faulting on the island of Crete (Greece). *Geophysical Journal International*, *183*(1), 111–126. https://doi.org/10.1111/j.1365-246X.2010.04749.x

Caputo, R., Chatzipetros, A., Pavlides, S., & Sboras, S. (2012). The Greek database of seismogenic sources (GreDaSS): State-of-the-art for northern Greece. *Annals of Geophysics*, *55*(5), 859–894. https://doi.org/10.4401/ag-5168

Caputo, R., & Pavlides, S. (1993). Late Cainozoic geodynamic evolution of Thessaly and surroundings (central-northern Greece). *Tectonophysics*, *223*(3–4), 339–362. https://doi.org/10.1016/0040-1951(93)90144-9

Caroir, F., Chanier, F., Gaullier, V., Sakellariou, D., Bailleul, J., Maillard, A., et al. (2024). Late Quaternary deformation in the western extension of the North Anatolian Fault (North Evia, Greece): Insights from very high-resolution seismic data (WATER surveys). *Tectonophysics*, *870*, 230138. https://doi.org/10.1016/j.tecto.2023.230138

Chatzipetros, A., Kiratzi, A., Sboras, S., Zouros, N., & Pavlides, S. (2013). Active faulting in the north-eastern Aegean Sea Islands. *Tectonophysics*, *597–598*, 106–122. https://doi.org/10.1016/j.tecto.2012.11.026

Chousianitis, K. (2026). GPS velocities and earthquake slip vectors in the Aegean [Dataset]. *Zenodo*. https://doi.org/10.5281/zenodo.20268296

21699356, 2026, 7, Downloaded from https://agupubs.onlinelibrary.wiley.com/doi/10.1029/2025JB033218, Wiley Online Library on [04/07/2026]. See the Terms and Conditions (https://onlinelibrary.wiley.com/terms-and-conditions) on Wiley Online Library for rules of use; OA articles are governed by the applicable Creative Commons License

Chousianitis, K., Ganas, A., & Evangelidis, C. P. (2015). Strain and rotation rate patterns of mainland Greece from continuous GPS data and comparison between seismic and geodetic moment release. *Journal of Geophysical Research: Solid Earth*, *120*(5), 3909–3931. https://doi.org/10.1002/2014JB011762

Chousianitis, K., Ganas, A., & Gianniou, M. (2013). Kinematic interpretation of present-day crustal deformation in central Greece from continuous GPS measurements. *Journal of Geodynamics*, *71*, 1–13. https://doi.org/10.1016/j.jog.2013.06.004

Chousianitis, K., & Konca, A. O. (2018). Coseismic slip distribution of the 12 June 2017 Mw = 6.3 Lesvos earthquake and imparted static stress changes to the neighboring crust. *Journal of Geophysical Research: Solid Earth*, *123*(10), 8926–8936. https://doi.org/10.1029/2018JB015950

Chousianitis, K., Konca, A. O., Tselentis, G.-A., Papadopoulos, G. A., & Gianniou, M. (2016). Slip model of the 17 November 2015 Mw = 6.5 Lefkada earthquake from the joint inversion of geodetic and seismic data. *Geophysical Research Letters*, *43*(15), 7973–7981. https://doi.org/10.1002/2016GL069764

Chousianitis, K., Özbey, V., Sboras, S., McCaffrey, R., & Ergintav, S. (2026). Block kinematics, interseismic coupling and fault slip rates in the Aegean region from GPS and earthquake slip vector data: 2. Hellenic subduction system. *Journal of Geophysical Research: Solid Earth*, *131*(7), e2025JB033219. https://doi.org/10.1029/2025JB033219

Chousianitis, K., Sboras, S., Mouslopoulou, V., Chouliaras, G., & Hristopulos, D. T. (2024). The upper crustal deformation field of Greece inferred from GPS data and its correlation with earthquake occurrence. *Journal of Geophysical Research: Solid Earth*, *129*(4), e2023JB028004. https://doi.org/10.1029/2023JB028004

Clarke, P. J., Davies, R. R., England, P. C., Parsons, B., Billiris, H., Paradissis, D., et al. (1998). Crustal strain in central Greece from repeated GPS measurements in the interval 1989–1997. *Geophysical Journal International*, *135*(1), 195–214. https://doi.org/10.1046/j.1365-246X.1998.00633.x

Clews, J. E. (1989). Structural controls on basin evolution: Neogene to Quaternary of the Ionian zone, Western Greece. *Journal of the Geological Society*, *146*(3), 447–457. https://doi.org/10.1144/gsjgs.146.3.0447

Coffey, K. T., Ingersoll, R. V., & Schmitt, A. K. (2019). Stratigraphy, provenance, and tectonic significance of the Punchbowl block, San Gabriel Mountains, California, USA. *Geosphere*, *15*(2), 479–501. https://doi.org/10.1130/GES02025.1

Cundy, A. B., Gaki-Papanastassiou, K., Papanastassiou, D., Maroukian, H., Frogley, M. R., & Cane, T. (2010). Geological and geomorphological evidence of recent coastal uplift along a major Hellenic normal fault system (the Kamena Vourla fault zone, NW Evoikos Gulf, Greece). *Marine Geology*, *271*(1–2), 156–164. https://doi.org/10.1016/j.margeo.2010.02.009

Dewey, J. F., & Şengör, A. M. C. (1979). Aegean and surrounding regions: Complex multiplate and continuum tectonics in a convergent zone. *Geological Society of America Bulletin*, *90*(1), 84–92. https://doi.org/10.1130/0016-7606(1979)90<84:aasrcm>2.0.co;2

DISS Working Group. (2018). Database of Individual Seismogenic Sources (DISS), version 3.2.1: A compilation of potential sources for earthquakes larger than M 5.5 in Italy and surrounding areas. https://doi.org/10.6092/INGV.IT-DISS3.2.1

Eliet, P. P., & Gawthorpe, R. L. (1995). Drainage development and sediment supply within rifts, examples from the Sperchios basin, central Greece. *Journal of the Geological Society*, *152*(5), 883–893. https://doi.org/10.1144/gsjgs.152.5.0883

Elitez, İ., Yaltırak, C., & Aktuğ, B. (2016). Extensional and compressional regime driven left-lateral shear in southwestern Anatolia (eastern Mediterranean): The Burdur-Fethiye Shear Zone. *Tectonophysics*, *688*, 26–35. https://doi.org/10.1016/j.tecto.2016.09.024

Ergintav, S., Floyd, M., Paradissis, D., Karabulut, H., Vernant, P., Masson, F., et al. (2022). New geodetic constraints on the role of faults and blocks versus distributed strain in the nubia-arabia-eurasia zone of active plate interactions. *Turkish Journal of Earth Sciences*, *32*(3), 248–261. https://doi.org/10.55730/1300-0985.1842

Evangelidis, C., & Fountoulakis, I. (2023). Imaging the Western edge of the aegean shear Zone: The South Evia 2022-2023 seismic sequence. *Seismica*, *2*(1). https://doi.org/10.26443/seismica.v2i1.1032

Evelpidou, N., Pirazzoli, P. A., Vassilopoulos, A., & Tomasin, A. (2011). Holocene submerged shorelines on Theologos area (Greece). *Zeitschrift für Geomorphologie*, *55*(1), 31–44. https://doi.org/10.1127/0372-8854/2011/0055-0032

Feng, L. J., Newman, A. V., Farmer, G. T., Psimoulis, P., & Stiros, S. C. (2010). Energetic rupture, coseismic and post-seismic response of the 2008 Mw 6.4 Achaia-Elia Earthquake in northwestern Peloponnese, Greece: An indicator of an immature transform fault zone. *Geophysical Journal International*, *183*(1), 103–110. https://doi.org/10.1111/j.1365-246X.2010.04747.x

Floyd, M., Billiris, H., Paradissis, D., Veis, G., Avallone, A., Briole, P., et al. (2010). A new velocity field for Greece: Implications for the kinematics and dynamics of the Aegean. *Journal of Geophysical Research*, *115*(B10), B10403. https://doi.org/10.1029/2009JB007040

Fountoulis, I., Mariolakos, I., & Ladas, I. (2014). Quaternary basin sedimentation and geodynamics in SW Peloponnese (Greece) and late stage uplift of Taygetos Mt. *Bollettino di Geofisica Teorica ed Applicata*, *55*(2), 303–324.

Gaki-Papanastassiou, K., Karymbalis, E., Papanastassiou, D., & Maroukian, H. (2009). Quaternary marine terraces as indicators of neotectonic activity of the Ierapetra normal fault SE Crete (Greece). *Geomorphology*, *104*(1–2), 38–46. https://doi.org/10.1016/j.geomorph.2008.05.037

Ganas, A., Marinou, A., Anastasiou, D., Paradissis, D., Papazissi, K., Tzavaras, P., & Drakatos, G. (2013). GPS-derived estimates of crustal deformation in the central and north Ionian Sea, Greece: 3-yr results from NOANET continuous network data. *Journal of Geodynamics*, *67*, 62–71. https://doi.org/10.1016/j.jog.2012.05.010

Gessner, K., Gallardo, L. A., Markwitz, V., Ring, U., & Thomson, S. N. (2013). What caused the denudation of the Menderes Massif: Review of crustal evolution, lithosphere structure, and dynamic topography in southwest Turkey. *Gondwana Research*, *24*(1), 243–274. https://doi.org/10.1016/j.gr.2013.01.005

Goldsworthy, M., & Jackson, J. (2001). Migration of activity within normal fault systems: Examples from the Quaternary of mainland Greece. *Journal of Structural Geology*, *23*(2–3), 489–506. https://doi.org/10.1016/S0191-8141(00)00121-8

Goldsworthy, M., Jackson, J., & Haines, J. (2002). The continuity of active fault systems in Greece. *Geophysical Journal International*, *148*(3), 596–618. https://doi.org/10.1046/j.1365-246X.2002.01609.x

Haddad, A., Ganas, A., Kassaras, I., & Lupi, M. (2020). Seismicity and geodynamics of western Peloponnese and central Ionian Islands: Insights from a local seismic deployment. *Tectonophysics*, *778*, 228353. https://doi.org/10.1016/j.tecto.2020.228353

Halpaap, F., Rondenay, S., & Ottemöller, L. (2018). Seismicity, deformation, and metamorphism in the Western Hellenic subduction zone. New constraints from tomography. *Journal of Geophysical Research: Solid Earth*, *123*(4), 3000–3026. https://doi.org/10.1002/2017JB015154

Hatzfeld, D., Besnard, M., Makropoulos, K., & Hatzidimitriou, P. (1993). Microearthquake seismicity and fault-plane solutions in the southern Aegean and its geodynamic implications. *Geophysical Journal International*, *115*(3), 799–818. https://doi.org/10.1111/j.1365-246X.1993.tb01493.x

Hatzfeld, D., Karakostas, V., Ziazia, M., Kassaras, I., Papadimitriou, E., Makropoulos, K., et al. (2000). Microseismicity and faulting geometry in the Gulf of Corinth (Greece). *Geophysical Journal International*, *141*(2), 438–456. https://doi.org/10.1046/j.1365-246x.2000.00092.x

Hatzfeld, D., Martinod, J., Bastet, G., & Gautier, P. (1997). An analog experiment for the Aegean to describe the contribution of gravitational potential energy. *Journal of Geophysical Research*, *102*(B1), 649–659. https://doi.org/10.1029/96JB02594

21699356, 2026, 7, Downloaded from https://agupubs.onlinelibrary.wiley.com/doi/10.1029/2025JB033218, Wiley Online Library on [04/07/2026]. See the Terms and Conditions (https://onlinelibrary.wiley.com/terms-and-conditions) on Wiley Online Library for rules of use; OA articles are governed by the applicable Creative Commons License

Hatzfeld, D., Ziazia, M., Kementzetzidou, D., Hatzidimitriou, P., Panagiotopoulos, D., Makropoulos, K., et al. (1999). Microseismicity and focal mechanisms at the western termination of the North Anatolian Fault and their implications for continental tectonics. *Geophysical Journal International*, *137*(3), 891–908. https://doi.org/10.1046/j.1365-246x.1999.00851.x

Hempton, M. R. (1982). The North Anatolian fault and complexities of continental escape. *Journal of Structural Geology*, *4*(4), 502–504. https://doi.org/10.1016/0191-8141(82)90041-4

Hollenstein, C., Muller, M. D., Geiger, A., & Kahle, H.-G. (2008). Crustal motion and deformation in Greece from a decade of GPS measurements, 1993–2003. *Tectonophysics*, *449*(1–4), 17–40. https://doi.org/10.1016/j.tecto.2007.12.006

Hooft, E. E., Nomikou, P., Toomey, D. R., Lampridou, D., Getz, C., Christopoulou, M. E., et al. (2017). Backarc tectonism, volcanism, and mass wasting shape seafloor morphology in the santorini-christiana-amorgos region of the Hellenic Volcanic Arc. *Tectonophysics*, *712*, 396–414. https://doi.org/10.1016/j.tecto.2017.06.005

Howell, A., Jackson, J., Copley, A., McKenzie, D., & Nissen, E. (2017). Subduction and vertical coastal motions in the eastern Mediterranean. *Geophysical Journal International*, *211*(1), 593–620. https://doi.org/10.1093/gji/ggx307

Howell, A., Jackson, J., England, P., Higham, T., & Synolakis, C. (2015). Late Holocene uplift of Rhodes, Greece: Evidence for a large tsunamigenic earthquake and the implications for the tectonics of the eastern Hellenic Trench System. *Geophysical Journal International*, *203*(1), 459–474. https://doi.org/10.1093/gji/ggv307

Jackson, J., & McKenzie, D. (1984). Active tectonics of the Alpine-Himalayan belt between western Turkey and Pakistan. *Geophysical Journal International*, *77*(1), 185–264. https://doi.org/10.1111/j.1365-246X.1984.tb01931.x

Jenny, S., Goes, S., Giardini, D., & Kahle, H.-G. (2004). Earthquake recurrence parameters from seismic and geodetic strain rates in eastern Mediterranean. *Geophysical Journal International*, *157*(3), 1331–1347. https://doi.org/10.1111/j.1365-246X.2004.02261.x

Kahle, H.-G., Cocard, M., Peter, Y., Geiger, A., Reilinger, R., Barka, A., & Veis, G. (2000). GPS-derived strain rate field within the boundary zones of the Eurasian, African, and Arabian Plates. *Journal of Geophysical Research*, *105*(B10), 23353–23370. https://doi.org/10.1029/2000JB900238

Kapetanidis, V., & Kassaras, I. (2019). Contemporary crustal stress of the Greek region deduced from earthquake focal mechanisms. *Journal of Geodynamics*, *123*, 55–82. https://doi.org/10.1016/j.jog.2018.11.004

Karabulut, H., Schmittbuhl, J., Özalaybey, S., Lengliné, O., Kömeç-Mutlu, A., Durand, V., et al. (2011). Evolution of the seismicity in the eastern Marmara Sea a decade before and after the 17 August 1999 Izmit earthquake. *Tectonophysics*, *510*(1–2), 17–27. https://doi.org/10.1016/j.tecto.2011.07.009

Kassaras, I., Kapetanidis, V., & Karakonstantis, A. (2016). On the spatial distribution of seismicity and the 3D tectonic stress field in western Greece. *Physics and Chemistry of the Earth*, *95*, 50–72. https://doi.org/10.1016/j.pce.2016.03.012

Keraudren, B., & Sorel, D. (1987). The terraces of Corinth (Gerrce) - A detailed record of eustatic sea-level variations during the last 500,000 years. *Marine Geology*, *77*(1–2), 99–107. https://doi.org/10.1016/0025-3227(87)90085-5

Kilias, A. A., Tranos, M. D., Papadimitriou, E. E., & Karakostas, V. G. (2008). The recent crustal deformation of the Hellenic orogen in Central Greece; the Kremasta and Sperchios Fault Systems and their relationship with the adjacent large structural features. *Zeitschrift der Deutschen Gesellschaft fur Geowissenschaften*, *159*(3), 533–547. https://doi.org/10.1127/1860-1804/2008/0159-0533

Kiratzi, A., & Louvari, E. (2003). Focal mechanisms of shallow earthquakes in the Aegean Sea and the surrounding lands determined by waveform modelling: A new database. *Journal of Geodynamics*, *36*(1–2), 251–274. https://doi.org/10.1016/S0264-3707(03)00050-4

Kokinou, E., Kamberis, E., Vafidis, A., Monopolis, D., Ananiadis, G., & Zelilidis, A. (2005). Deep seismic reflection data from offshore western Greece: A new crustal model for the Ionian Sea. *Journal of Petroleum Geology*, *28*(2), 185–202. https://doi.org/10.1111/j.1747-5457.2005.tb00079.x

Konstantinou, K. I., Mouslopoulou, V., Liang, W.-T., Heidbach, O., Oncken, O., & Suppe, J. (2017). Present-day crustal stress field in Greece inferred from regional-scale damped inversion of earthquake focal mechanisms. *Journal of Geophysical Research: Solid Earth*, *122*(1), 506–523. https://doi.org/10.1002/2016JB013272

Kreemer, C., & Chamot-Rooke, N. (2004). Contemporary kinematics of the southern Aegean and the Mediterranean Ridge. *Geophysical Journal International*, *157*(3), 1377–1392. https://doi.org/10.1111/j.1365-246X.2004.02270.x

Kreemer, C., Chamot-Rooke, N., & Le Pichon, X. (2004). Constraints on the evolution and vertical coherency of deformation in the Northern Aegean from a comparison of geodetic, geologic and seismologic data. *Earth and Planetary Science Letters*, *225*(3–4), 329–346. https://doi.org/10.1016/j.epsl.2004.06.018

Kurt, A. I., Özbakir, A. D., Cingoz, A., Ergintav, S., Dogan, U., & Özarpaci, S. (2023). Contemporary velocity field for Turkey inferred from combination of a dense network of long term GNSS observations. *Turkish Journal of Earth Sciences*, *32*(3), 275–293. https://doi.org/10.55730/1300-0985.1844

Lambotte, S., Lyon-Caen, H., Bernard, P., Deschamps, A., Patau, G., Nercessian, A., et al. (2014). Reassessment of the rifting process in the Western Corinth Rift from relocated seismicity. *Geophysical Journal International*, *197*(3), 1822–1844. https://doi.org/10.1093/gji/ggu096

Lazos, I., Papanikolaou, I., Sboras, S., Foumelis, M., & Pikridas, C. (2022). Geodetic upper crust deformation based on primary GNSS and INSAR data in the Strymon Basin, Northern greece-correlation with active faults. *Applied Sciences*, *12*(18), 9391. https://doi.org/10.3390/app12189391

Le Pichon, X., & Angelier, J. (1979). The Hellenic arc and trench system: A key to the neotectonic evolution of the eastern Mediterranean area. *Tectonophysics*, *60*(1–2), 1–42. https://doi.org/10.1016/0040-1951(79)90131-8

Le Pichon, X., Chamot-Rooke, N., Lallemant, S., Noomen, R., & Veis, G. (1995). Geodetic determination of the kinematics of central Greece with respect to Europe: Implications for eastern Mediterranean tectonics. *Journal of Geophysical Research*, *100*(B7), 12675–12690. https://doi.org/10.1029/95JB00317

Le Pichon, X., & Gaulier, J.-M. (1988). The rotation of Arabia and the Levant fault system. *Tectonophysics*, *153*(1–4), 271–294. https://doi.org/10.1016/0040-1951(88)90020-0

Le Pichon, X., & Kreemer, C. (2010). The miocene-to-present kinematic evolution of the Eastern mediterranean and Middle East and its implications for dynamics. *Annual Review of Earth and Planetary Sciences*, *38*(1), 323–351. https://doi.org/10.1146/annurev-earth-040809-152419

Little, T. A., & Jones, A. (1998). Seven million years of strike-slip and related off-fault deformation, northeastern Marlborough fault system, South Island, New Zealand. *Tectonics*, *17*(2), 285–302. https://doi.org/10.1029/97TC03148

Louvari, E., Kiratzi, A., Papazachos, B., & Hatzidimitriou, P. (2001). Fault-plane solutions determined by waveform modeling confirm tectonic collision in the eastern Adriatic. *Pure and Applied Geophysics*, *158*(9), 1613–1637. https://doi.org/10.1007/PL00001236

Lyon-Caen, H., Armijo, R., Drakopoulos, J., Baskoutas, J., Delibassis, N., Gaulon, R., et al. (1988). The 1986 Kalamata (South Peloponnesus) earthquake: Detailed study of a normal fault, evidences for east-west extension in the Hellenic Arc. *Journal of Geophysical Research*, *93*(B12), 14967–15000. https://doi.org/10.1029/JB093iB12p14967

21699356, 2026, 7, Downloaded from https://agupubs.onlinelibrary.wiley.com/doi/10.1029/2025JB033218, Wiley Online Library on [04/07/2026]. See the Terms and Conditions (https://onlinelibrary.wiley.com/terms-and-conditions) on Wiley Online Library for rules of use; OA articles are governed by the applicable Creative Commons License

21699356, 2026, 7, Downloaded from https://agupubs.onlinelibrary.wiley.com/doi/10.1029/2025JB033218, Wiley Online Library on [04/07/2026]. See the Terms and Conditions (https://onlinelibrary.wiley.com/terms-and-conditions) on Wiley Online Library for rules of use; OA articles are governed by the applicable Creative Commons License

Makropoulos, K., Kaviris, G., & Kouskouna, V. (2012). An updated and extended earthquake catalogue for Greece and adjacent areas since 1900. *Natural Hazards and Earth System Sciences*, *12*(5), 1425–1430. https://doi.org/10.5194/nhess-12-1425-2012

Martinod, J., Hatzfeld, D., Brun, J. P., Davy, P., & Gautier, P. (2000). Continental collision, gravity spreading, and kinematics of Aegea and Anatolia. *Tectonics*, *19*(2), 290–299. https://doi.org/10.1029/1999TC900061

McCaffrey, R. (2002). Crustal block rotations and plate coupling. In S. Stein & J. T. Freymueller (Eds.), *Plate boundary zones, geodynamic series*, *Geodynamics Series* (Vol. 30, pp. 101–119). https://doi.org/10.1029/GD030p0101

McCaffrey, R. (2005). Block kinematics of the Pacific-North America plate boundary in the southwestern United States from inversion of GPS, seismological and geologic data. *Journal of Geophysical Research*, *110*(B7), B07401. https://doi.org/10.1029/2004JB003307

McCaffrey, R. (2009). Time-dependent inversion of three-component continuous GPS for steady and transient sources in northern Cascadia. *Geophysical Research Letters*, *36*(7), L07304. https://doi.org/10.1029/2008GL036784

McCaffrey, R. (2023). Tdefnode [Software]. *Github*. Retrieved from https://robmccaffrey.github.io/TDEFNODE/TDEFNODE.html

McCaffrey, R., Qamar, A. I., King, R. W., Wells, R., Khazaradze, G., Williams, C. A., et al. (2007). Fault locking, block rotation and crustal deformation in the Pacific Northwest. *Geophysical Journal International*, *169*(3), 1315–1340. https://doi.org/10.1111/j.1365-246X.2007.03371.x

McClusky, S., Balassanian, S., Barka, A., Demir, C., Ergintav, S., Georgiev, I., et al. (2000). Global positioning system constraints on plate kinematics and dynamics in the eastern Mediterranean and Caucasus. *Journal of Geophysical Research*, *105*(B3), 5695–5719. https://doi.org/10.1029/1999JB900351

McKenzie, D. (1972). Active tectonics of the Mediterranean region. *Geophysical Journal International*, *30*(2), 109–185. https://doi.org/10.1111/j.1365-246X.1972.tb02351.x

McKenzie, D. (1978). Active tectonics of the Alpine-Himalayan belt: The Aegean Sea and surrounding regions. *Geophysical Journal International*, *55*(1), 217–254. https://doi.org/10.1111/j.1365-246X.1978.tb04759.x

McNeill, L. C., Mille, A., Minshull, T. A., Bull, J. M., Kenyon, N. H., & Ivanov, M. (2004). Extension of the North Anatolian Fault into the North Aegean Trough: Evidence for transtension, strain partitioning, and analogues for Sea of Marmara basin models. *Tectonics*, *23*(2), TC2016. https://doi.org/10.1029/2002TC001490

Mechernich, S., Reicherter, K., Deligiannakis, G., & Papanikolaou, I. (2023). Tectonic geomorphology of active faults in Eastern Crete (Greece) with slip rates and earthquake history from cosmogenic ^{36}Cl dating of the Lastros and Orno faults. *Quaternary International*, *651*, 77–91. https://doi.org/10.1016/j.quaint.2022.04.007

Mercier, J. L., Sorel, D., Vergely, P., & Simeakis, K. (1989). Extensional tectonic regimes in the Aegean basins during the Cenozoic. *Basin Research*, *2*(1), 49–71. https://doi.org/10.1111/j.1365-2117.1989.tb00026.x

Merryman Boncori, J. P., Papoutsis, I., Pezzo, G., Tolomei, C., Atzori, S., Ganas, A., et al. (2015). The February 2014 Cephalonia earthquake (Greece): 3D deformation field and source modeling from multiple SAR techniques. *Seismological Research Letters*, *86*(1), 124–137. https://doi.org/10.1785/0220140126

Moretti, I., Sakellariou, D., Lykousis, V., & Micarelli, L. (2003). The Gulf of Corinth: An active half graben? *Journal of Geodynamics*, *36*(1–2), 323–340. https://doi.org/10.1016/S0264-3707(03)00053-X

Nicol, A., Mouslopoulou, V., Begg, J., & Oncken, O. (2020). Displacement accumulation and sampling of paleoearthquakes on active normal faults of Crete in the eastern Mediterranean. *Geochemistry, Geophysics, Geosystems*, *21*(11), e2020GC009265. https://doi.org/10.1029/2020GC009265

Nissen, E., Cambaz, M. D., Gaudreau, É., Howell, A., Karasözen, E., & Savidge, E. (2022). A reappraisal of active tectonics along the Fethiye-Burdur trend, Southwestern Turkey. *Geophysical Journal International*, *230*(2), 1030–1051. https://doi.org/10.1093/gji/ggac096

Nomikou, P., Hübscher, C., Papanikolaou, D., Farangitakis, G. P., Ruhnau, M., & Lampridou, D. (2018). Expanding extension, subsidence and lateral segmentation within the Santorini-Amorgos basins during Quaternary: Implications for the 1956 Amorgos events, central-south Aegean Sea, Greece. *Tectonophysics*, *722*, 138–153. https://doi.org/10.1016/j.tecto.2017.10.016

Nyst, M., & Thatcher, W. (2004). New constraints on the active tectonic deformation of the Aegean. *Journal of Geophysical Research*, *109*(B11), B11406. https://doi.org/10.1029/2003JB002830

Okada, Y. (1992). Internal deformation due to shear and tensile faults in a half-space. *Bulletin of the Seismological Society of America*, *82*(2), 1018–1040. https://doi.org/10.1785/BSSA0820021018

Özbakır, A. D., Govers, R., & Fichtner, A. (2020). The Kefalonia Transform Fault: A STEP fault in the making. *Tectonophysics*, *787*, 228471. https://doi.org/10.1016/j.tecto.2020.228471

Özbakır, A. D., Sengör, A. M. C., Wortel, M. J. R., & Govers, R. (2013). The Pliny-Strabo trench region: A large shear zone resulting from slab tearing. *Earth and Planetary Science Letters*, *375*, 188–195. https://doi.org/10.1016/j.epsl.2013.05.025

Özbey, V., Özeren, M. S., Henry, P., Elliot, K., Galgana, G., Karabulut, H., et al. (2021). Kinematics of the Marmara Region: A fusion of continuum and block models. *Mediterranean Geoscience Reviews*, *3*(1), 57–78. https://doi.org/10.1007/s42990-021-00051-y

Özkaptan, M., Kaymakci, N., Langereis, C. G., Gulyuz, E., Özacar, A. A., Uzel, B., & Sözbilir, H. (2018). Age and kinematics of the Burdur Basin: Inferences for the existence of the Fethiye Burdur Fault Zone in SW Anatolia (Turkey). *Tectonophysics*, *744*, 256–274. https://doi.org/10.1016/j.tecto.2018.07.009

Palyvos, N., Bantekas, I., & Kranis, H. (2006). Transverse fault zones of subtle geomorphic signature in northern Evia island (central Greece extensional province): An introduction to the Quaternary Nileas graben. *Geomorphology*, *76*(3–4), 363–374. https://doi.org/10.1016/j.geomorph.2005.12.002

Pantosti, D., De Martini, P. M., Papanastassiou, D., Lemeille, F., Palyvos, N., & Stavrakakis, G. (2004). Paleoseismological trenching across the atalanti fault (Central Greece): Evidence for the ancestors of the 1894 earthquake during the Middle Ages and roman times. *Bulletin of the Seismological Society of America*, *94*(2), 531–549. https://doi.org/10.1785/0120020207

Papadopoulos, G. A., & Pavlides, S. B. (1992). The large 1956 earthquake in the South Aegean: Macroseismic field configuration, faulting, and neotectonics of Amorgos Island. *Earth and Planetary Science Letters*, *113*(3), 383–396. https://doi.org/10.1016/0012-821X(92)90140-Q

Papanastassiou, D., Cundy, A. B., Gaki-Papanastassiou, K., Frogley, M. R., Tsanakas, K., & Maroukian, H. (2014). The uplifted terraces of the Arkitsa region, NW Evoikos Gulf, Greece: A result of combined tectonic and volcanic processes? *The Journal of Geology*, *122*(4), 397–410. https://doi.org/10.1086/676595

Papanastassiou, D., Gaki-Papanastassiou, K., & Maroukian, H. (2005). Recognition of past earthquakes along the Sparta fault (Peloponnesus, southern Greece) during the Holocene, by combining results of different dating techniques. *Journal of Geodynamics*, *40*(2–3), 189–199. https://doi.org/10.1016/j.jog.2005.07.015

Papanikolaou, D., Lykousis, V., Chronis, G., & Pavlakis, P. (1988). A comparative study of neotectonic basins across the Hellenic arc: The Messiniakos, Argolikos, Saronikos and Southern Evoikos Gulfs. *Basin Research*, *1*(3), 167–176. https://doi.org/10.1111/j.1365-2117.1988.tb00013.x

Papanikolaou, I., Dafnis, P., Deligiannakis, G., Hengesh, J., & Panagopoulos, A. (2022). Active faults, Paleoseismological trenching and seismic hazard assessment in the Northern Mygdonia Basin, Northern Greece: The Assiros-Krithia fault and the Drimos fault zone. *Quaternary International*, *651*, 92–107. https://doi.org/10.1016/j.quaint.2022.02.001

Papazachos, B., & Papazachou, C. (2003). *The earthquakes of Greece, 3rd edition*. Editions Ziti. [in Greek].286

Papoulia, J., & Makris, J. (2004). Microseismicity and active deformation of Messinia, SW Greece. *Journal of Seismology*, *8*(4), 439–451. https://doi.org/10.1007/s10950-004-4837-1

Pavlides, S., Mountrakis, D., Kilias, A., & Tranos, M. (1990). The role of strike-slip movements in the extensional area of Northern Aegean (Greece). A case of transtensional tectonics. *Annales Tectonicae*, *4*(2), 196–211.

Pavlides, S. B., & Kilias, A. A. (1987). Neotectonic and active faults along the Serbomacedonian zone (SE Chalkidiki, northern Greece). *Annales Tectonicae*, *1*(2), 97–104.

Pavlides, S. B., & Sboras, S. (2021). Recent earthquake activity of March 2021 in Northern Thessaly unlocks new scepticism on faults. *Turkish Journal of Earth Sciences*, *30*(8), 851–861. https://doi.org/10.3906/yer-2110-6

Pearce, F. D., Rondenay, S., Sachpazi, M., Charalampakis, M., & Royden, L. H. (2012). Seismic investigation of the transition from continental to oceanic subduction along the western Hellenic Subduction Zone. *Journal of Geophysical Research*, *117*(B7), B07306. https://doi.org/10.1029/2011JB009023

Perissoratis, C., & Papadopoulos, G. (1999). Sediment instability and slumping in the southern Aegean Sea and the case history of the 1956 tsunami. *Marine Geology*, *161*(2–4), 287–305. https://doi.org/10.1016/S0025-3227(99)00039-0

Perissoratis, C., & van Andel, T. H. (1991). Sea-level changes and tectonics in the Quaternary extensional basin of the South Evvoikos Gulf, Greece. *Terra Nova*, *3*(3), 294–302. https://doi.org/10.1111/j.1365-3121.1991.tb00147.x

Pérouse, E., Chamot-Rooke, N., Rabaute, A., Briole, P., Jouanne, F., Georgiev, I., & Dimitrov, D. (2012). Bridging onshore and offshore present-day kinematics of central and eastern Mediterranean: Implications for crustal dynamics and mantle flow. *Geochemistry, Geophysics, Geosystems*, *13*(9), Q09013. https://doi.org/10.1029/2012GC004289

Pérouse, E., Sébrier, M., Braucher, R., Chamot-Rooke, N., Bourlès, D., Briole, P., et al. (2017). Transition from collision to subduction in Western Greece: The Katouna–Stamna active fault system and regional kinematics. *International Journal of Earth Sciences*, *106*(3), 967–989. https://doi.org/10.1007/s00531-016-1345-9

Piper, D. J. W., & Perissoratis, C. (2003). Quaternary neotectonics of the South Aegean arc. *Marine Geology*, *198*(3–4), 259–288. https://doi.org/10.1016/S0025-3227(03)00118-X

Pondrelli, S. (2002). European-Mediterranean regional centroid-moment tensors catalog (RCMT) [Dataset]. Istituto Nazionale di Geofisica e Vulcanologia (INGV). https://doi.org/10.13127/rcmt/euromed

Porkoláb, K., Willingshofer, E., Sokoutis, D., Békési, E., & Beekman, F. (2023). Post-5 Ma rock deformation on Alonnisos (Greece) constrains the propagation of the North Anatolian Fault. *Tectonophysics*, *846*, 229654. https://doi.org/10.1016/j.tecto.2022.229654

Poulimenos, G., & Doutsos, T. (1997). Flexural uplift of rift flanks in central Greece. *Tectonics*, *16*(6), 912–923. https://doi.org/10.1029/97TC01658

Reilinger, R., McClusky, S., Vernant, P., Lawrence, S., Ergintav, S., Cakmak, R., et al. (2006). GPS constraints on continental deformation in the Africa-Arabia-Eurasia continental collision zone and implications for the dynamics of plate interactions. *Journal of Geophysical Research*, *111*(B5), B05411. https://doi.org/10.1029/2005JB004051

Rigo, A., Lyon-Caen, H., Armijo, R., Deschamps, A., Hatzfeld, D., Makropoulos, K., et al. (1996). A microseismic study in the western part of the Gulf of Corinth (Greece): Implications for large-scale normal faulting mechanisms. *Geophysical Journal International*, *126*(3), 663–688. https://doi.org/10.1111/j.1365-246X.1996.tb04697.x

Roberts, G. P., & Ganas, A. (2000). Fault-slip directions in central and southern Greece measured from striated and corrugated fault planes: Comparison with focal mechanism and geodetic data. *Journal of Geophysical Research*, *105*(B10), 23443–23462. https://doi.org/10.1029/1999JB900440

Roberts, S., & Jackson, J. (1991). Active normal faulting in central Greece: An overview. *Geological Society, London, Special Publications*, *56*(1), 125–142. https://doi.org/10.1144/GSL.SP.1991.056.01.09

Rodriguez, M., Sakellariou, D., Gorini, C., Janin, A., D'Acremont, E., Le Pourhiet, L., et al. (2023). Evolution of the North Anatolian Fault from a diffuse to a localized shear zone in the North Aegean Sea during the Plio-Pleistocene. *Geophysical Journal International*, *235*(3), 2614–2639. https://doi.org/10.1093/gji/ggad364

Roussos, N., & Lyssimachou, T. (1991). Structure of the Central North Aegean Trough: An active strike-slip deformation zone. *Basin Research*, *3*(1), 37–46. https://doi.org/10.1111/j.1365-2117.1991.tb00134.x

Royden, L. H. (1993). The tectonic expression slab pull at continental convergent boundaries. *Tectonics*, *12*(2), 303–325. https://doi.org/10.1029/92TC02248

Savage, J. C., & Burford, R. O. (1973). Geodetic determination of relative plate motion in central California. *Journal of Geophysical Research*, *78*(5), 832–845. https://doi.org/10.1029/JB078i005p00832

Sboras, S. (2011). The Greek database of seismogenic sources: Seismotectonic implications for North Greece (PhD Thesis, University of Ferrara). *Pubblicazioni dello IUSS*, *5*(1), 252.

Sboras, S., Chatzipetros, A., & Pavlides, S. (2017). North Aegean active fault pattern and the 24 May 2014, Mw 6.9 earthquake. In I. Çemen & Y. Yilmaz (Eds.), *Active global seismology: Neotectonics and earthquake potential of the Eastern Mediterranean Region*, *Geophysical Monograph 225* (pp. 239–272). John Wiley and Sons Inc. https://doi.org/10.1002/9781118944998.ch9

Sboras, S., Lazos, I., Bitharis, S., Pikridas, C., Galanakis, D., Fotiou, A., et al. (2021). Source modelling and stress transfer scenarios of the October 30, 2020 Samos earthquake: Seismotectonic implications. *Turkish Journal of Earth Sciences*, *30*(8), 699–717. https://doi.org/10.3906/yer-2107-25

Sboras, S., Mouzakiotis, E., Chousianitis, K., Karastathis, V., Evangelidis, C., Lazos, I., et al. (2025). Where does the active North Aegean Sea shear stop? Geodynamic and seismotectonic implications from recent strike-slip earthquake occurrences and GPS-based geodetic analysis in Euboea, Phthiotis and Boeotia, Central Greece. *Tectonophysics*, *914*, 230917. https://doi.org/10.1016/j.tecto.2025.230917

Sboras, S., Pavlides, S., Kilias, A., Galanakis, D., Chatziioannou, A., & Chatzipetros, A. (2022). The geological structure and tectonic complexity of Northern Thessaly that hosted the March 2021 seismic crisis. *Geotechnics*, *2*(4), 935–960. https://doi.org/10.3390/geotechnics2040044

Şengör, A. M. C. (1979). The North Anatolian transform fault: Its age, offset and tectonic significance. *Journal of the Geological Society*, *136*(3), 269–282. https://doi.org/10.1144/gsjgs.136.3.0269

Şengör, A. M. C., & Canitez, N. (1982). The north Anatolian fault, in Alpine Mediterranean Geodynamics. In H. Berckhemer & K. Hsü (Eds.), *Geodynamics series* (Vol. 7, pp. 205–216). AGU. https://doi.org/10.1029/GD007p0205

Shaw, B., & Jackson, J. (2010). Earthquake mechanisms and active tectonics of the Hellenic subduction zone. *Geophysical Journal International*, *181*, 966–984. https://doi.org/10.1111/j.1365-246X.2010.04551.x

21699356, 2026, 7, Downloaded from https://agupubs.onlinelibrary.wiley.com/doi/10.1029/2025JB033218, Wiley Online Library on [04/07/2026]. See the Terms and Conditions (https://onlinelibrary.wiley.com/terms-and-conditions) on Wiley Online Library for rules of use; OA articles are governed by the applicable Creative Commons License

Sorel, D. (2000). A Pleistocene and still-active detachment fault and the origin of the Corinth-Patras rift, Greece. *Geology*, *28*(1), 83–86. https://doi.org/10.1130/0091-7613(2000)028<0083:apasad>2.3.co;2

Sözbilir, H., Sarı, B., Uzel, B., Sümer, Ö., & Akkiraz, S. (2011). Tectonic implications of transtensional supradetachment basin development in an extension-parallel transfer zone: The Kocaçay Basin, western Anatolia, Turkey. *Basin Research*, *23*(4), 423–448. https://doi.org/10.1111/j.1365-2117.2010.00496.x

Sparacino, F., Galuzzi, B. G., Palano, M., Segou, M., & Chiarabba, C. (2022). Seismic coupling for the aegean-anatolian region. *Earth-Science Reviews*, *228*, 103993. https://doi.org/10.1016/j.earscirev.2022.103993

Taylor, B., Weiss, J. R., Goodliffe, A. M., Sachpazi, M., Laigle, M., & Hirn, A. (2011). The structures, stratigraphy and evolution of the Gulf of Corinth rift, Greece. *Geophysical Journal International*, *185*(3), 1189–1219. https://doi.org/10.1111/j.1365-246X.2011.05014.x

Taymaz, T., Jackson, J., & McKenzie, D. (1991). Active tectonics of the north and central Aegean Sea. *Geophysical Journal International*, *106*(2), 433–490. https://doi.org/10.1111/j.1365-246X.1991.tb03906.x

Taymaz, T., Jackson, J., & Westaway, R. (1990). Earthquake mechanisms in the Hellenic Trench near Crete. *Geophysical Journal International*, *102*(3), 695–731. https://doi.org/10.1111/j.1365-246X.1990.tb04590.x

Tiryakioğlu, İ., Floyd, M., Erdoğan, S., Gülal, E., Ergintav, S., McClusky, S., & Reilinger, R. (2013). GPS constraints on active deformation in the Isparta Angle region of SW Turkey. *Geophysical Journal International*, *195*(3), 1455–1463. https://doi.org/10.1093/gji/ggt323

Tsampouraki-Kraounaki, K., Sakellariou, D., Rousakis, G., Morfis, I., Panagiotopoulos, I., Livanos, I., et al. (2021). The Santorini-Amorgos Shear Zone: Evidence for dextral transtension in the South Aegean back-arc Region, Greece. *Geosciences*, *11*(5), 216. https://doi.org/10.3390/geosciences11050216

Underhill, J. R. (1989). Late Cenozoic deformation of the Hellenide foreland, western Greece. *Geological Society of America Bulletin*, *101*(5), 613–634. https://doi.org/10.1130/0016-7606(1989)101<0613:lcdoth>2.3.co;2

Valkaniotis, S., Briole, P., Ganas, A., Elias, P., Kapetanidis, V., Tsironi, V., et al. (2020). The Mw = 5.6 Kanallaki earthquake of 21 March 2020 in West Epirus, Greece: Reverse fault model from InSAR data and seismotectonic implications for Apulia-Eurasia collision. *Geosciences*, *10*(11), 454. https://doi.org/10.3390/geosciences10110454

van Andel, T. H., Perissoratis, C., & Rondoyanni, T. (1993). Quaternary tectonics of the Argolikos Gulf and adjacent basins, Greece. *Journal of the Geological Society*, *150*(3), 529–539. https://doi.org/10.1144/gsjgs.150.3.0529

Vassilakis, E., Royden, L., & Papanikolaou, D. (2011). Kinematic links between subduction along the Hellenic trench and extension in the Gulf of Corinth, Greece: A multidisciplinary analysis. *Earth and Planetary Science Letters*, *303*(1–2), 108–120. https://doi.org/10.1016/j.epsl.2010.12.054

Veliz, V., Mouslopoulou, V., Nicol, A., Fassoulas, C., Begg, J., & Oncken, O. (2018). Millennial to million year normal-fault interactions in the forearc of a subduction margin, Crete, Greece. *Journal of Structural Geology*, *113*, 225–241. https://doi.org/10.1016/j.jsg.2018.05.019

Vernant, P., Reilinger, R., & McClusky, S. (2014). Geodetic evidence for low coupling on the Hellenic subduction plate interface. *Earth and Planetary Science Letters*, *385*, 122–129. https://doi.org/10.1016/j.epsl.2013.10.018

Wallace, L. M., Beavan, J., McCaffrey, R., & Darby, D. (2004). Subduction zone coupling and tectonic block rotations in the North Island, New Zealand. *Journal of Geophysical Research*, *109*(B12), B12406. https://doi.org/10.1029/2004JB003241

Wallace, L. M., McCaffrey, R., Beavan, J., & Ellis, S. (2005). Rapid microplate rotations and back-arc rifting at the transition between collision and subduction. *Geology*, *33*(11), 857–860. https://doi.org/10.1130/G21834.1

Wardell, N., Camera, L., Mascle, J., Nicolich, R., Marchi, M., & Barison, E. (2014). The structural framework of the Peloponnese continental margin from Zakynthos to Pylos from seismic reflection and morpho-bathymetric data. *Bollettino di Geofisica Teorica ed Applicata*, *55*(2), 343–367.

Wessel, P., Luis, J. F., Uieda, L., Scharroo, R., Wobbe, F., Smith, W. H. F., & Tian, D. (2019). The generic mapping tools version 6. *Geochemistry, Geophysics, Geosystems*, *20*(11), 5556–5564. https://doi.org/10.1029/2019GC008515

Whittaker, A. C., & Walker, A. S. (2015). Geomorphic constraints on fault throw rates and linkage times: Examples from the Northern Gulf of Evia, Greece. *Journal of Geophysical Research, Earth Surface*, *120*(1), 137–158. https://doi.org/10.1002/2014JF003318

Woodside, J., Mascle, J., Huguen, C., & Volkonskaia, A. (2000). The Rhodes Basin, a Post-Miocene tectonic trough. *Marine Geology*, *165*(1–4), 1–12. https://doi.org/10.1016/S0025-3227(99)00140-1

Yaltırak, C., & Alpar, B. (2002). Kinematics and evolution of the northern branch of the North Anatolian Fault (Ganos Fault) between the Sea of Marmara and the Gulf of Saros. *Marine Geology*, *190*(1–2), 351–366. https://doi.org/10.1016/S0025-3227(02)00354-7

References From the Supporting Information

Calais, E., DeMets, C., & Nocquet, J. M. (2003). Evidence for a post-3.16-Ma change in nubia-eurasia-north America plate motions. *Earth and Planetary Science Letters*, *216*(1–2), 81–92. https://doi.org/10.1016/S0012-821X(03)00482-5

D'Agostino, N., Avallone, A., Cheloni, D., D'Anastasio, E., Mantenuto, S., & Selvaggi, G. (2008). Active tectonics of the Adriatic region from GPS and earthquake slip vectors. *Journal of Geophysical Research*, *113*(B12), B12413. https://doi.org/10.1029/2008JB005860

DeMets, C., Gordon, R. G., & Argus, D. F. (2010). Geologically current plate motions. *Geophysical Journal International*, *181*(1), 1–80. https://doi.org/10.1111/j.1365-246X.2009.04491.x

Di Giacomo, D., Engdahl, E. R., & Storchak, D. A. (2018). The ISC-GEM Earthquake Catalogue (1904–2014): Status after the Extension Project. *Earth System Science Data*, *10*(4), 1877–1899. https://doi.org/10.5194/essd-10-1877-2018

McClusky, S., Reilinger, R., Mahmoud, S., Ben Sari, D., & Tealeb, A. (2003). GPS constraints on Africa (Nubia) and Arabia plate motions. *Geophysical Journal International*, *155*(1), 126–138. https://doi.org/10.1046/j.1365-246X.2003.02023.x

Stein, S., & Gordon, R. G. (1984). Statistical tests of additional plate boundaries from plate motion inversions. *Earth and Planetary Science Letters*, *69*(2), 401–412. https://doi.org/10.1016/0012-821X(84)90198-5

Storchak, D., Di Giacomo, D., Bondár, I., Engdahl, E. R., Harris, J., Lee, W. H. K., et al. (2013). Public release of the ISC-GEM global instrumental earthquake catalogue (1900-2009). *Seismological Research Letters*, *84*(5), 810–815. https://doi.org/10.1785/0220130034

Storchak, D., Di Giacomo, D., Engdahl, E., Harris, J., Bondár, I., Lee, W., et al. (2015). The ISC-GEM global instrumental earthquake catalogue (1900-2009): Introduction. *Physics of the Earth and Planetary Interiors*, *239*, 48–63. https://doi.org/10.1016/j.pepi.2014.06.009

21699356, 2026, 7, Downloaded from https://agupubs.onlinelibrary.wiley.com/doi/10.1029/2025JB033218, Wiley Online Library on [04/07/2026]. See the Terms and Conditions (https://onlinelibrary.wiley.com/terms-and-conditions) on Wiley Online Library for rules of use; OA articles are governed by the applicable Creative Commons License